BACHELOR OF INDUSTRIAL TECHNOLOGY ENGINEERING

BACHELOR'S FINAL PROJECT

VIRTUAL SYNCHRONOUS MACHINES PROVIDING INERTIA IN LOW-INERTIA RES POWER SYSTEMS

Author: Emilio Juan Valdivielso Suárez

Director: Lukas Sigrist

Madrid

Declaro, bajo mi responsabilidad, que el Proyecto presentado con el título

MÁQUINAS SÍNCRONAS VIRTUALES PROPORCIONANDO INERCIA EN SISTEMAS DE RES DE BAJA INERCIA

en la ETS de Ingeniería - ICAI de la Universidad Pontificia Comillas en el

curso académico 2022/23 es de mi autoría, original e inédito y

no ha sido presentado con anterioridad a otros efectos.

El Proyecto no es plagio de otro, ni total ni parcialmente y la información que ha sido

tomada de otros documentos está debidamente referenciada.

Fdo.: Emilio Juan Valdivielso Suárez Fecha: …5…/ …07…/ …2023…

Autorizada la entrega del proyecto

EL DIRECTOR DEL PROYECTO

Fdo.: Lukas Sigrist Fecha: …5…/ …07…/ …2023…

BACHELOR OF INDUSTRIAL TECHNOLOGY ENGINEERING

BACHELOR'S FINAL PROJECT

VIRTUAL SYNCHRONOUS MACHINES PROVIDING INERTIA IN LOW-INERTIA RES POWER SYSTEMS

Author: Emilio Juan Valdivielso Suárez

Director: Lukas Sigrist

Madrid

MÁQUINAS SÍNCRONAS VIRTUALES PROPORCIONANDO INERCIA EN SISTEMAS DE RES DE BAJA INERCIA

Autor: Valdivielso Suárez, Emilio Juan.
Director: Sigrist, Lukas.
Entidad Colaboradora: ICAI – Universidad Pontificia Comillas

RESUMEN DEL PROYECTO

En este proyecto se ha diseñado un control de frecuencia tipo VSM para un modelo de convertidor grid forming implementado en Matlab/Simulink con el objetivo de estudiar el comportamiento de la inercia virtual que presenta este tipo de convertidores frente a la inercia real de una máquina síncrona convencional. Además, en este estudio se pretende entender el comportamiento de esta respuesta inercial sintética cuando se alcanzan los límites de corriente del convertidor.

Palabras clave: Grid Formig, VSM, Droop

1. Introducción

El aumento en la introducción de energías renovables en la red, especialmente en microrredes, y la sustitución de las máquinas síncronas convencionales por estas, ha llevado inevitablemente a una disminución de la inercia global del sistema. Esta disminución de la inercia hace que las redes sean más sensibles a cambios en la potencia pudiendo llevar a la inestabilidad del sistema. Con el objetivo de evitar este problema surge el convertidor grid forming con control VSM que permite fijar una tensión en la red y establecer una frecuencia imitando el comportamiento de la máquina síncrona en cuanto a respuesta inercial se refiere.

2. Definición del proyecto

El proyecto consiste en la elaboración de un control de frecuencia tipo VSM para un modelo de convertidor grid forming implementado en Matlab/Simulink con el objetivo de poder hacer un estudio de la respuesta inercial sintética que presenta este tipo de convertidor tanto en condiciones normales de operación como cuando se alcanza el límite de corriente del convertidor. Para ello primero se ha realizado un acercamiento teórico al problema y posteriormente se ha puesto a prueba la teoría estudiando la respuesta del convertidor ante diferentes fallos en la red, cuando opera en solitario y cuando interactúa con una máquina síncrona haciendo uso de un modelo de red implementado en Simulink.

3. Descripción del modelo/sistema/herramienta

El sistema empleado para el estudio consiste en una microrred que incluye una máquina síncrona y un convertidor grid forming en el lado de baja tensión y una carga puramente

resistiva y una fuente de tensión trifásica en el lado de alta tensión, tal y como se muestra en la Figura 1.

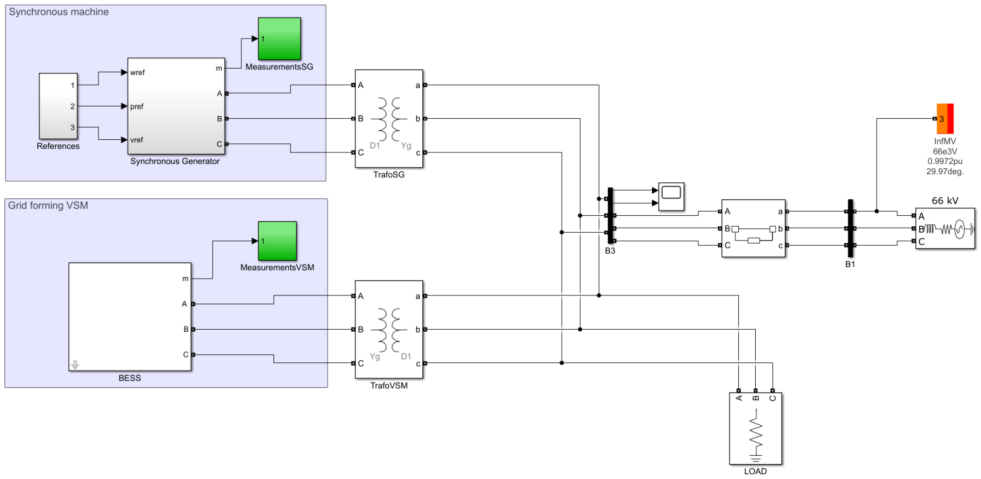

Figura 1:Modelo de la microrred

La idea es simular la perdida de la fuente de tensión trifásica para poder estudiar la respuesta inercial del convertidor y la máquina síncrona ante el desequilibrio de potencia. Para ello se ha diseñado en Simulink un control tipo VSM que sigue la ecuación de swing de la máquina síncrona cuyo esquema aparece en la Figura 2.

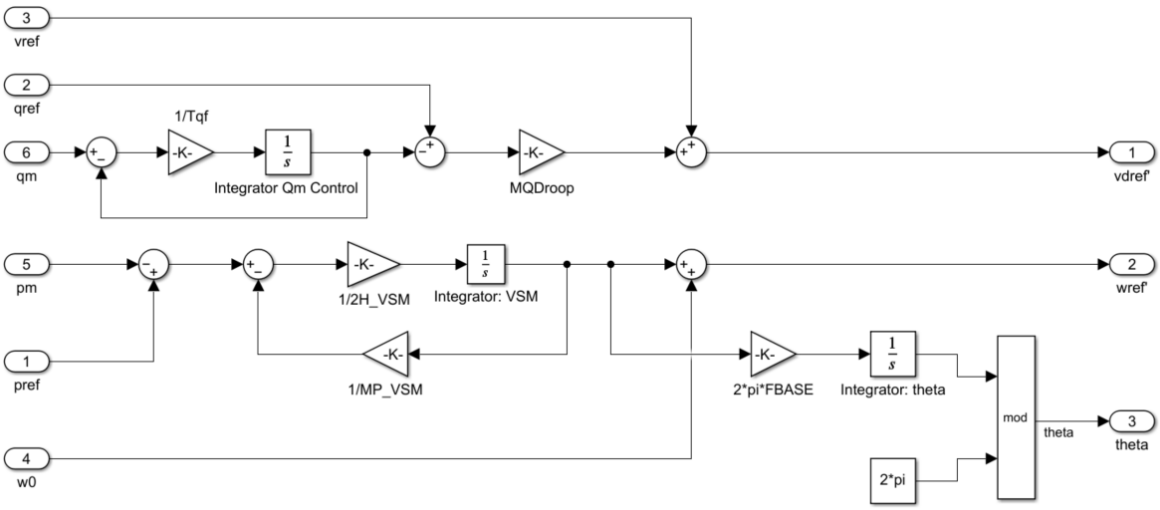

Figura 2: Control de frecuencia VSM y control de tensión por estatismo

El control VSM se ha diseñado a partir del modelo de control droop equivalente que lleva a la ecuación (1), que describe el comportamiento inercial de una máquina síncrona ante una variación en la potencia de la red. La equivalencia entre ambos controles se explica en [1].

$$2H \cdot \frac{d\omega}{dt} = p_m - p_e - D_{SM}(\omega - 1) \quad (1)$$

Con el fin de entender el comportamiento inercial del convertidor se han realizado 3 ensayos para 3 configuraciones de red diferentes, cuyos resultados ante condiciones estándar y ante condiciones límite de funcionamiento del convertidor, se resumen y se muestran en el siguiente apartado. En la configuración 1 sólo regula el convertidor, en la configuración 2 regulan el convertidor y una máquina síncrona, y en la configuración 3 regulan dos máquinas síncronas haciendo una de ellas las veces de convertidor funcionando con los mismos valores de estatismo e inercia que este.

4. Resultados

- **En condiciones normales de funcionamiento:**

  El convertidor presenta una respuesta inercial muy similar a la de la máquina síncrona incluso con valores más favorables de RoCoF y frecuencia nadir (frecuencia mínima) tal y como se puede ver en Tabla 1, Tabla 2, Tabla 3 y Tabla 4. Las tablas 1 y 2 muestran los resultados para la configuración 2 y las tablas 3 y 4 para la configuración 3. Si comparamos los valores de RoCoF del convertidor de la Tabla 1 con los valores de RoCoF del generador síncrono "SG1" de la Tabla 3, podemos observar que para mismos valores de la constante de inercia el convertidor presenta una respuesta con menos pendiente máxima. Es decir, para mismos valores de constante de inercia el convertidor parece responder mejor ante la misma perturbación cuando trabaja sin alcanzar el límite de corriente.

H_{VSM} (s)	$\lvert RoCoF_{VSM}\rvert_{MAX}$(pu/s)	$Nadir_{SG}$
2	$31.41*10^{-3}$	0.996327
4	$18.46*10^{-3}$	0.996545
6	$13.10*10^{-3}$	0.996585
8	$10.16*10^{-3}$	0.996535
10	$8.30*10^{-3}$	0.996475
12	$7*10^{-3}$	0.996416
14	$6.01*10^{-3}$	0.996367

Tabla 1: RoCoF máximo en valor absoluto del convertidor y frecuencia nadir del generador.

$\|RoCoF_{SG}\|_{t=1^+}$(pu/s)	$Nadir_{VSM}$ (pu)	f_{ss} (pu)
$20.77*10^{-3}$	0.996673	0.996673

Tabla 2: RoCoF del SG en el instante del fallo, frecuencia nadir del convertidor y frecuencia en régimen permanente.

H_{VSM} (s)	$\|RoCoF\|_{MAX,SG1}$(pu/s)	$\|RoCoF\|_{MAX,SG}$(pu/s)	$Nadir_{SG1}$	$Nadir_{SG}$
2	$46.11*10^{-3}$	$21.7*10^{-3}$	0.994659	0.993895
4	$23.06*10^{-3}$	$17.05*10^{-3}$	0.995529	0.994491
6	$15.34*10^{-3}$	$15.71*10^{-3}$	0.995907	0.994917
8	$11.44*10^{-3}$	$15.32*10^{-3}$	0.996069	0.995328
10	$9.18*10^{-3}$	$15.17*10^{-3}$	0.996121	0.99569
12	$7.65*10^{-3}$	$15.10*10^{-3}$	0.996171	0.995987
14	$6.49*10^{-3}$	$15.07*10^{-3}$	0.996235	0.996209

Tabla 3: RoCoF máximo en valor absoluto y frecuencia nadir de ambos generadores síncronos.

$\|RoCoF_{SG}\|_{t=1^+}$(pu/s)	f_{ss} (pu)
$14.67*10^{-3}$	0.996637

Tabla 4: RoCoF del SG en el instante del fallo y frecuencia en régimen permanente.

- **En condiciones límite de funcionamiento:**

  Si el convertidor alcanza el límite de corriente que puede circular por los transistores el comportamiento inercial no desaparece, pero el convertidor es incapaz de regular correctamente la tensión en el condensador provocando un comportamiento como el mostrado en la Figura 3. Esta figura presenta la frecuencia virtual del convertidor para diferentes escenarios de carga de este, cuando se le aplica un escalón de potencia igual en todos los casos. Es decir, se pierde una generación que aportaba 5MW a la red. Se puede observar que pese a ser el mismo escalón de potencia la respuesta inercial depende de lo cerca que este el límite de corriente de las condiciones de trabajo antes del fallo. Esto se debe a que el convertidor cada vez dispone de menos margen de corriente para poder regular la tensión haciendo que la potencia demandada disminuya cuadráticamente con esta. Por este motivo podemos ver que la frecuencia del convertidor presenta un escalón menor cuanto antes se alcanza el límite de corriente. Para que el estudio tenga sentido se ha escogido un escenario en

el que el convertidor limita, pero es capaz de mantener una tensión en la red aceptable. En concreto se ha escogido el caso en el que la carga es de 28 MW.

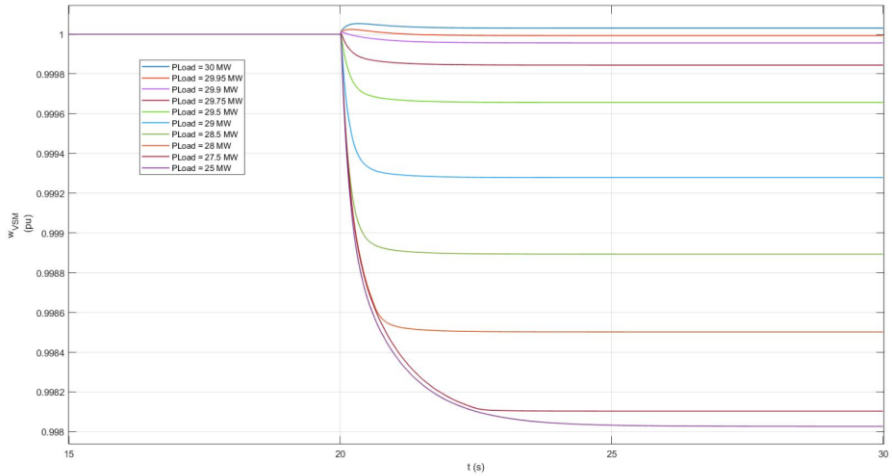

Figura 3: Frecuencia del convertidor para condiciones límite de corriente.

Simulando este escenario para diferentes valores de la constante de inercia del convertidor se han obtenido los resultados de RoCoF máximo mostrados en la Tabla 5. Si comparamos estos resultados con los obtenidos en la Tabla 1, correspondientes al convertidor trabajando en condiciones normales, podemos ver que el RoCoF es menor para mismos valores de inercia cuando el convertidor satura, lo cual es lógico teniendo en cuenta que la variación de potencia disminuye cuadráticamente con el valor de tensión inicial que el convertidor no consigue regular cuando alcanza el límite.

H_{VSM} (s)	$\|RoCoF\|_{MAX}$ (pu/s)
2	$19.1*10^{-3}$
4	$10.89*10^{-3}$
6	$7.63*10^{-3}$
8	$5.88*10^{-3}$
10	$4.78*10^{-3}$
12	$4.02*10^{-3}$
14	$3.49*10^{-3}$

Tabla 5: RoCoF máximo en valor absoluto.

5. Conclusiones

Este trabajo pretendía implementar un control VSM en Matlab/Simulink y analizar la respuesta inercial del convertidor frente a perturbaciones en la red cuando el convertidor trabaja en condiciones normales y cuando llega al límite de corriente.

Con este propósito se ha diseñado un control VSM en Simulink y se han simulado diferentes configuraciones de convertidores Grid Forming y máquinas síncronas para distintas perturbaciones en la red. Estas simulaciones han consistido en aislar el convertidor sólo o junto con la máquina síncrona de la red para que alimente una carga puramente resistiva.

Estos objetivos se han cumplido y se ha llegado a las siguientes conclusiones:

- Como se ha podido comprobar la inercia virtual funciona correctamente cuando el convertidor opera en condiciones normales, tiene un funcionamiento similar al de una máquina síncrona presentando incluso un RoCoF menos pronunciado para los mismos valores de inercia.
- Cuando se alcanza el límite de corriente del convertidor la respuesta inercial no desaparece, pero se ve afectada por la imposibilidad del convertidor de regular la tensión de la red. Dando lugar a un problema adyacente, que es la dependencia del convertidor de regular la tensión del condensador para proporcionar una respuesta inercial similar a la de una máquina síncrona convencional. Además, como consecuencia de la limitación del convertidor la respuesta de la frecuencia deja de parecerse tanto a una respuesta propia de un sistema de primer orden presentando un codo brusco en su pendiente.
- La inercia virtual del convertidor Grid Forming con control VSM depende en gran medida del control de tensión del condensador del filtro LC. Esto puede suponer un problema si el convertidor llega al límite de corriente cuando alimenta cargas invariantes ante la tensión.

6. Referencias

[1] S. D'Arco and J. A. Suul, "Equivalence of Virtual Synchronous Machines and Frequency-Droops for Converter-Based MicroGrids," in IEEE Transactions on Smart Grid, vol. 5, no. 1, pp. 394-395, Jan. 2014, doi: 10.1109/TSG.2013.228800.

VIRTUAL SYNCHRONOUS MACHINES PROVIDING INERTIA IN LOW-INERTIA RES POWER SYSTEMS

Author: Valdivielso Suárez, Emilio Juan.
Supervisor: Sigrist, Lukas.
Collaborating Entity: ICAI – Universidad Pontificia Comillas

ABSTRACT

In this project, a VSM-type frequency control has been designed for a grid-forming converter model implemented in Matlab/Simulink, with the aim of studying the behavior of the virtual inertia exhibited by this type of converter compared to the real inertia of a conventional synchronous machine. Additionally, this study aims to understand the behavior of this synthetic inertia response when the converter's current limits are reached.

Keywords: Grid Forming, VSM, Droop.

1. Introduction

The increased integration of renewable energies into the grid, especially in microgrids, and the replacement of conventional synchronous machines by them, has inevitably led to a decrease in the overall system inertia. This decrease in inertia makes the networks more sensitive to power changes, which can lead to system instability. To avoid this problem, the grid-forming converter with VSM control has been developed, which allows setting a voltage in the grid and establishing a frequency that mimics the behavior of a synchronous machine in terms of inertia response.

2. Project Definition

The project consists of developing a VSM-type frequency control for a grid-forming converter model implemented in Matlab/Simulink, with the aim of studying the synthetic inertia response exhibited by this type of converter under normal operating conditions and when the converter's current limit is reached. To achieve this, a theoretical approach to the problem was first carried out, and then the theory was tested by studying the converter's response to different faults in the grid, both when operating independently and when interacting with a synchronous machine using a network model implemented in Simulink.

3. Description of the Model/System/Tool

The system used for the study consists of a microgrid that includes a synchronous machine and a grid-forming converter on the low-voltage side, and a purely resistive load and a three-phase voltage source on the high-voltage side, as shown in Figure 1.

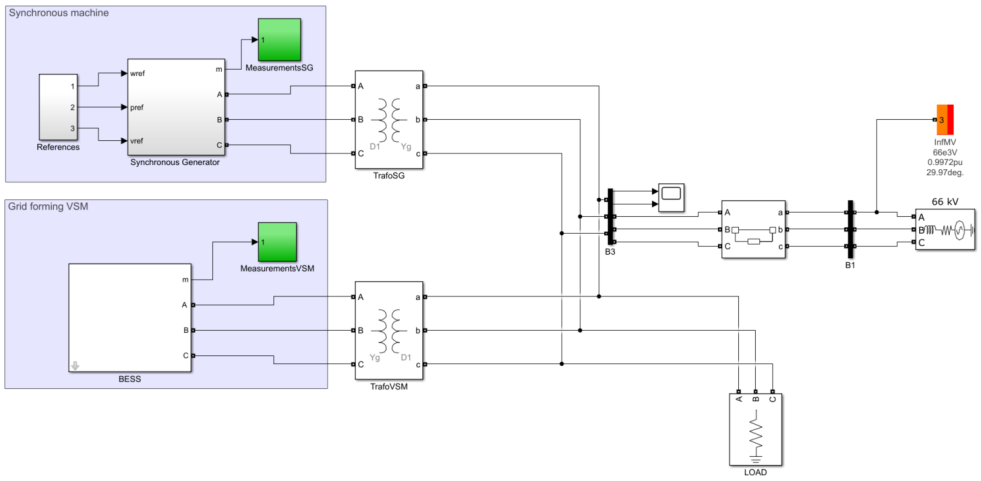

Figure 1:Model of microgrid system

The purpose is to simulate the loss of the three-phase voltage source in order to study the inertia response of the converter and the synchronous machine in the face of power imbalance. To achieve this, a VSM-type control has been designed in Simulink that follows the swing equation of the synchronous machine, as shown in Figure 2.

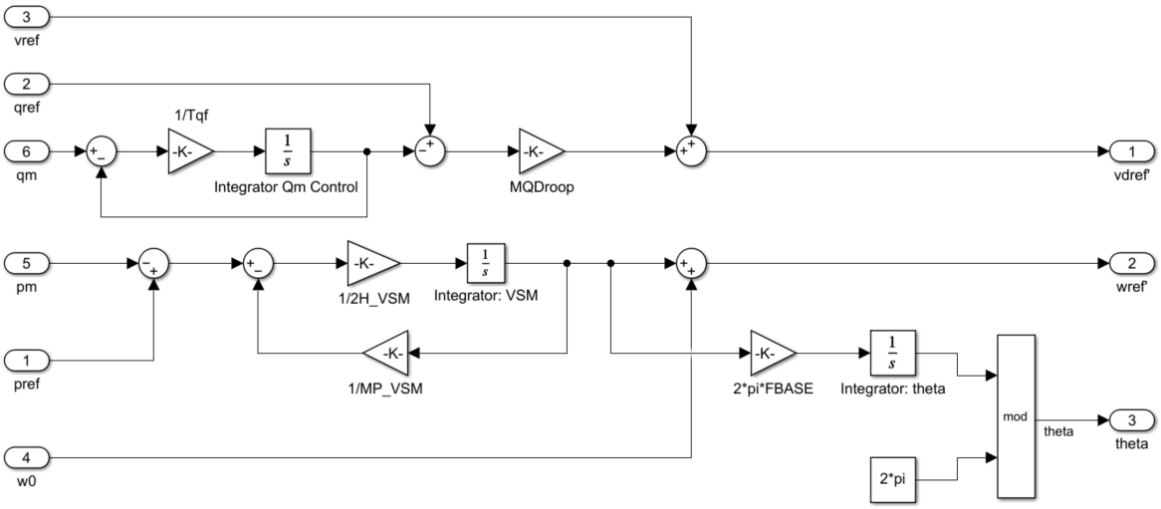

Figure 2: VSM frequency control and voltage droop control model

The VSM control has been designed based on the equivalent droop control model, which leads to the swing equation, seen in (1), that describes the inertia behavior of a synchronous machine in response to a power variation in the grid. The equivalence between both controls is explained in [1].

$$2H \cdot \frac{d\omega}{dt} = p_m - p_e - D_{SM}(\omega - 1) \quad (1)$$

In order to understand the inertial behavior of the converter, 3 tests have been performed for 3 different grid configurations, the results of which are summarized and shown in the following section for standard conditions and for converter operating limit conditions. In configuration 1, only the converter is involved in the primary regulation. In configuration 2, both the converter and a synchronous machine are involved. And in configuration 3, two synchronous machines are involved, with one of them acting as a converter, operating with the same droop and inertia values.

4. Results

- **Under normal operating conditions:**

  The converter exhibits a very similar response to that of the synchronous machine, even with more favorable values of rate of change of frequency (RoCoF) and frequency nadir (minimum frequency), as shown in Table 1, Table 2, Table 3 and Table 4. Tables 1 and 2 show the results for configuration 2 and tables 3 and 4 for configuration 3. If we compare the RoCoF values of the converter in Table 1 with the RoCoF values of the synchronous generator "SG1" shown in Table 3, we can observe that for the same values of the inertia constant the converter presents a response with a lower maximum slope. That is, for the same values of inertia constant the converter seems to respond better to the same disturbance when working without reaching the current limit.

H_{VSM} (s)	$\lvert RoCoF_{VSM}\rvert_{MAX}$(pu/s)	$Nadir_{SG}$
2	$31.41*10^{-3}$	0.996327
4	$18.46*10^{-3}$	0.996545
6	$13.10*10^{-3}$	0.996585
8	$10.16*10^{-3}$	0.996535
10	$8.30223*10^{-3}$	0.996475
12	$7*10^{-3}$	0.996416
14	$6.01*10^{-3}$	0.996367

Table 1: Maximum RoCoF in absolute value of the converter and frequency nadir of the SG.

$\lvert RoCoF_{SG}\rvert_{t=1^+}$(pu/s)	$Nadir_{VSM}$ (pu)	f_{ss} (pu)
$20.77*10^{-3}$	0.996673	0.996673

Table 2: RoCoF of the SG at the instant of failure, frequency nadir of the converter and frequency in steady state.

H_{VSM} (s)	$\lvert RoCoF\rvert_{MAX,SG1}$(pu/s)	$\lvert RoCoF\rvert_{MAX,SG}$(pu/s)	$Nadir_{SG1}$	$Nadir_{SG}$
2	$46.11*10^{-3}$	$21.7*10^{-3}$	0.994659	0.993895
4	$23.06*10^{-3}$	$17.05*10^{-3}$	0.995529	0.994491
6	$15.34*10^{-3}$	$15.71*10^{-3}$	0.995907	0.994917
8	$11.44*10^{-3}$	$15.32*10^{-3}$	0.996069	0.995328
10	$9.18*10^{-3}$	$15.17*10^{-3}$	0.996121	0.99569
12	$7.65*10^{-3}$	$15.10*10^{-3}$	0.996171	0.995987
14	$6.49*10^{-3}$	$15.07*10^{-3}$	0.996235	0.996209

Table 3: Maximum RoCoF in absolute value and frequency nadir of both synchronous machines.

$\lvert RoCoF_{SG}\rvert_{t=1^+}$(pu/s)	f_{ss} (pu)
$14.67*10^{-3}$	0.996637

Table 4: RoCoF of SG at the instant of failure and frequency in steady state.

- **Under extreme operating conditions:**

  If the converter reaches the current limit that can flow through the transistors, the inertial behavior does not disappear, but the converter is unable to correctly regulate the voltage on the capacitor causing a behavior as shown in Figure 3. This figure shows the frequency of the converter for different load scenarios when an equal power step is applied in all cases. In other words, a generation that contributed 5 MW to the grid is lost. It can be observed that despite being the same power step, the inertial response depends on how close the current limit is to the operating conditions before the fault. This is due to the fact that the converter has less and less current margin to be able to regulate the voltage, making the demanded power decrease quadratically with it. For this reason, we can see that the frequency of the converter presents a smaller step the sooner the current limit is reached. To make the study meaningful, a scenario has been chosen in which the converter limits but is able to

maintain an acceptable voltage in the grid. Specifically, the case where the load is 28 MW has been chosen.

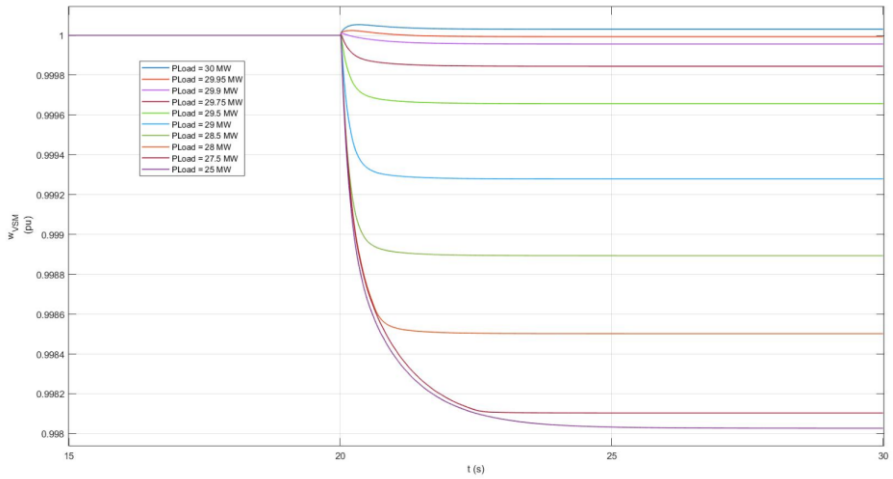

Figure 3: Frequency of the converter for current limit conditions

By simulating this scenario for different values of the converter inertia constant, the maximum RoCoF values shown in Table 5 have been obtained. If we compare these results with those obtained in Table 1, corresponding to the converter working under normal conditions, we can see that the RoCoF is lower for the same inertia values when the converter saturates, which is logical considering that the power variation decreases quadratically with the initial voltage value that the converter fails to regulate when it reaches the limit.

H_{VSM} (s)	$\|RoCoF\|_{MAX}$ (pu/s)
2	$19.1*10^{-3}$
4	$10.89*10^{-3}$
6	$7.63*10^{-3}$
8	$5.88*10^{-3}$
10	$4.78*10^{-3}$
12	$4.02*10^{-3}$
14	$3.49*10^{-3}$

Table 5: Maximum RoCoF in absolute value.

5. Conclusions

This work aimed to implement a VSM control in Matlab/Simulink and to analyze the inertial response of the converter against disturbances in the grid when the converter works under normal conditions and when it reaches the current limit.

For this purpose, a VSM control has been designed in Simulink and different configurations of Grid Forming converters and synchronous machines have been simulated for different disturbances in the grid. These simulations consisted of isolating the converter alone or together with the synchronous machine from the grid to feed a purely resistive load.

These objectives have been met and the following conclusions have been reached:

- As it has been verified the virtual inertia works correctly when the converter operates under normal conditions, it has a similar performance to a synchronous machine presenting even a flatter RoCoF for the same inertia values.
- When the current limit of the converter is reached the inertial response does not disappear but is affected by the converter's inability to regulate the grid voltage. Giving rise to an adjacent problem, which is the converter's dependence on regulating the capacitor voltage to provide an inertial response similar to that of a conventional synchronous machine. In addition, as a consequence of the converter limitation the frequency response ceases to resemble a first order system response and exhibits a sharp bend in its slope.
- The virtual inertia of the Grid Forming converter with VSM control is highly dependent on the voltage control of the LC filter capacitor. This can be a problem if the converter reaches the current limit when feeding voltage invariant loads.

6. References

[1] S. D'Arco and J. A. Suul, "Equivalence of Virtual Synchronous Machines and Frequency-Droops for Converter-Based MicroGrids," in IEEE Transactions on Smart Grid, vol. 5, no. 1, pp. 394-395, Jan. 2014, doi: 10.1109/TSG.2013.228800.

Index

Chapter 1. INTRODUCTION

1.1 INTRODUCTION

Frequency stability is concerned with the ability of generating units to supply their loads after a disturbance at a frequency within an acceptable range. Island power systems are especially sensitive to active power disturbances given their small size and their isolated character.

Currently, the frequency of the grid and its behavior due to variations in the load mainly depend on the inertia of the conventional Synchronous Machines (SM) and the primary frequency regulation. When a disruption occurs in the power balance of the grid, the SMs initially compensate for this energy imbalance between supply and demand by delivering or absorbing electrical energy in the form of kinetic energy that they accumulate in the rotor and which modifies rotor speed. The primary frequency regulation detects these rotor speed variations and it increases the power extracted from the primary resource.

Due to the increase in the use of renewable energy sources (solar or wind energy), there has been a decrease in the percentage of synchronous generators that participate in the primary regulation of frequency and contribute inertia to the grid, as SMs do.

These energy renewable sources are connected to the grid using electronic converters whose main objective until recently was to transfer to the grid the maximum amount of power arising from these sources.

This purpose is commonly achieved using a Grid Following control which allows regulating the amount of power transferred to the grid by controlling the converter current using a PLL (Phase Locked Loop) which synchronizes the phasor of the output voltage of the converter with the rotation of the d-q axis. This type of converter can be modeled as a controlled current

source and their main problem is that they need a grid imposing a voltage they can actually follow. This means that they cannot feed a passive load by controlling at the same time voltage and frequency, and they do not provide inertia inherently.

This decrease in the use of conventional generators providing inertia and participating in primary regulation leads to the use of batteries also connected to the grid through converters that are able to impose a voltage and that can regulate frequency similar to synchronous generators.

These types of converters are known as Grid Forming converters because they build a voltage at the output, so they do not need a strong grid that already provides a stable voltage. They are capable of powering a passive load in contrast to the Grid Following Converters.

There are different types of controllers used in these converters that allow them to contribute to the primary frequency regulation and emulate inertia. Their differences and characteristics have been widely discussed in the literature. Some control models examples are the Virtual Synchronous Machine (VSM), the Droop Control, and the VOC (Virtual Oscillator Control), all of them explained in [13].

In this project, we are going to focus on the operation of the converter with VSM control, which consists of implementing the motion equations of a real SM in the control, so that physically we have an electronic power converter, but theoretically it behaves like a synchronous machine.

However, the converters have limits, they present margins of current that cannot be exceeded. In fact, this is the problem that this project aims to solve. What happens if we reach those limits?

In a conventional SM, the inertia provided to the grid originates from the motion of the rotor, but the inertia generated by Grid Forming converters is control-based, which means that it is not physical. The literature suggests that this virtual inertia seems a good option as a

substitute for conventional inertia but the behavior of this control-based inertia when reaching the limits of the converter has not been explored in depth.

1.2 LITERATURE

In the literature it is possible to find different approaches on how to provide inertia to the grid and participate in primary regulation through Grid Forming converters.

Grid Forming converters are increasingly used in HVDC connections to isolated grids to avoid the reduction of total inertia of the system. Different schemes of Grid Forming Converters based on the droop control are studied in [1]. In this type of control a proportional compensation isa applied to the frequency and voltage output based on deviations from the reference values. The study of this control is performed with and without PLL with the aim of determining the advantages and disadvantages of using these controllers in the connection of HVDC systems. The results obtained in this study show that Grid Forming converters based on droop control are capable, depending on the design, of participating in the power active control, contributing to the primary frequency regulation and in the emulation of frequency. Demonstrating that the droop control scheme without PLL reduces the Rate of Change of Frequency (RoCoF) and increases the frequency nadir, in addition to avoiding problems related to instability caused by the PLL as explained in [3] and [4].

Nonetheless, as it has been addressed in the literature this scheme control without PLL loses one degree of freedom and it cannot guarantee the tracking of an active power reference due to its inherent participation in the primary frequency regulation. This means that the three functionalities of the control (frequency support, inertia emulation, and active power control) are coupled.

Despite that, a control scheme without PLL that allows the decoupling of the functionalities mentioned above is proposed in [2]. This control permits the owner of the converter to decide whether to participate or not in the primary frequency regulation.

The VSM was initially developed with the objective of emulating the behavior of a real SM by using its swing equation while the aim of the droop control was load sharing. But, as a result of introducing a low pass filter in the droop control to decouple its dynamics from the ones of inner loops, it can be shown in [6] that this filter allows the droop control to emulate inertia. Additionally, in [5], it is demonstrated that the droop control with low pass filter equations is equivalent to VSM equations under certain conditions. Specifically, in [8] it is shown that three conditions must be met: small frequency variations, constant active power reference, and constant frequency reference.

However, even if the aforementioned conditions are met, in [7] it is demonstrated that the droop and VSM models with equivalent constants according to the equations obtained in [5] present some issues. On one hand, the droop model has a low inertia effect while on the other hand, the VSM model has poor load-sharing capabilities. Furthermore, this equivalence is also studied in [9], where two conclusions are reached. The first one is that the transient responses of both controls are not equivalent, being the VSM model the one presenting more damped transients and less overshoot in response to load variations. And the second one is that the equivalence does not hold in steady–state for all values of inertia, damping, and short-circuit ratio. This means that although the droop model can be changed to its equivalent VSM model, as will be done in this project, the differences between both models and the advantages and disadvantages of this change must be taken into account.

1.3 OBJECTIVES OF THE PROJECT

The objectives that are intended to be achieved in this project are as follows:

- Implement a VSM control in MATLAB/Simulink.
- Simulate the response of the VSM control under different configuration and disturbances.
- Analyze the effect of converter limitations and in particular, current limitation, on the response of the VSM.

Chapter 2. VSM INVERTER MODELING

Before explaining the modeling that has been carried out in this project, it is necessary to make a small theoretical introduction of the grid forming converter and the modeling of the system on dq axes.

2.1 GRID FORMING CONVERTER

Grid forming converters, as opposed to grid following converters, impose a voltage and a frequency at their terminal. Although in the literature it is possible to find grid forming converter designs that make use of the PLL to estimate the grid frequency, here we are going to work with constant frequency and voltage references. For this, it is necessary to implement a power control, a voltage control and a current control.

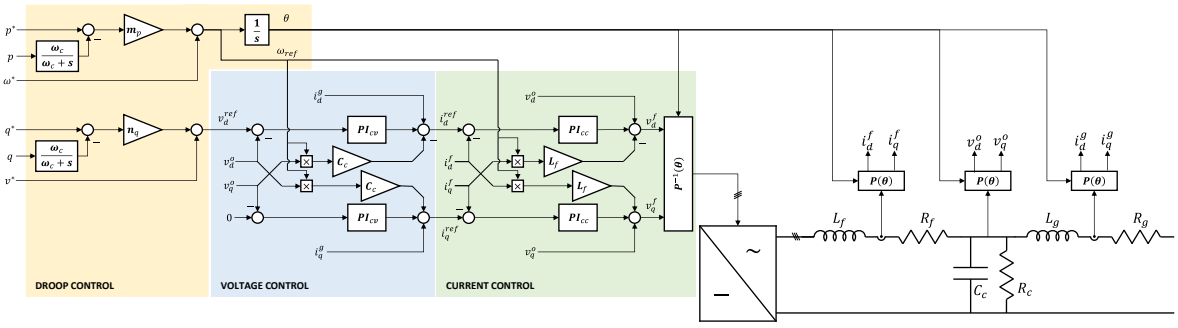

Figure 2.1: Grid Forming power, voltage and current control scheme seen in [14].

In Figure 2.1 we can see that the control structure is composed of three control stages: power control, voltage control and current control.

The control called droop control in the schematic has two functions:

The first one is to generate a reference frequency from the frequency setpoint by regulating the active power flow of the converter and also generating the angle to be used for the Park's transformation.

And the second one is to generate a reference voltage for the voltage control from a voltage setpoint and the reactive power flow.

The next control is the voltage control that can be generally defined as a PI control that is responsible for following the voltage reference obtained by the droop control and aims to generate the current reference of the converter.

The last control is the current control also implemented as a PI whose function is to generate the voltage reference of the converter thus allowing to control both the voltage at the capacitor and the power flow of the converter.

The controls summarized in this section will be discussed in more detail in *sections 2.3* and *2.4* below.

2.2 MODELING OF THE SYSTEM ON DQ AXES

In order to control a balanced three-phase system we usually work on a special system reference frame that allows us to treat the three-phase sinusoidal components as constants. For this purpose, the Clarke-Park transform is usually used. The Clarke-Park transform is divided into two stages, first the Clarke transform and then the Park transform.

The Clarke transform is a change of basis which makes it possible to go from a rotating three-dimensional voltage vector, whose projections on the A, B and C axes represent the voltage in each phase, to a two-dimensional vector which is also rotating. This transformation is made possible by a change of plane, this new plane being the one containing the three-dimensional vector. Being a balanced three-phase system, the plane in question is the plane that satisfies the implicit equation VA + VB + VC = 0.

Thus, the new reference frame commonly known in the literature as αβ, allows us to represent the rotating vector V_{ABC} = [VA, VB, VC] on some ABC axes as a rotating vector $V_{\alpha\beta}$ = [V_α, V_β] on αβ axes. This means that we now have two components with sinusoidal behavior.

Park's transform consists of establishing a reference system that rotates at the same angular velocity as the grid frequency so that instead of seeing two sine components on αβ axes, we now see two constant components on new axes commonly referred to as dq axes, so that we now have one vector V_{dq} = [V_d, V_q].

What is done to make the rotation of the dq axes of a particular converter independent of the rest, is to define a reference system independent of the rotation of the real voltage and current phasors. In the case of the model studied in this work we have established dq axes rotating at a frequency *wref* of 1 pu, i.e., 50 Hz. What we do when integrating the frequency is to obtain the park angle theta which advances or delays the measured voltage and current phasors so that they are seen as constants on the reference axes.

2.3 VOLTAGE AND CURRENT CONTROL LOOPS

The capacitor voltage control is performed by a decoupled cascade control that is composed of a current inner loop and a voltage outer loop. The control design is based on the voltage and current differential equations of the LC filter responsible for filtering the harmonics shown in Figure 2.2.

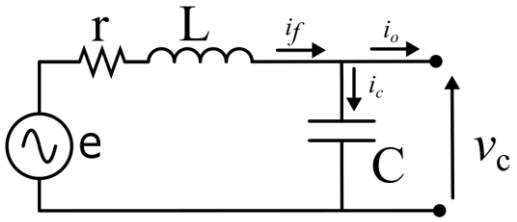

Figure 2.2: single-line diagram of the LC Filter at the converter output.

Differential equation of current control in pu:

$$e - v_c - r \times i_f = L \frac{di_f}{dt} \tag{2.1}$$

Differential equation of voltage control in pu:

$$i_f - i_o = C \frac{dV_c}{dt} \tag{2.2}$$

2.3.1 IMPLEMENTATION OF THE INNER CURRENT LOOP

To implement the inner current loop, the dq-axis differential equations obtained by performing the Clarke-Park transform to equation (2.1) are used.

The equations obtained on dq axes in pu are as follows:

$$e_d - v_{cd} - r \times i_{fd} + L \times \omega \times i_{fq} = \frac{L}{\Omega} \frac{di_{fd}}{dt} \tag{2.3}$$

$$e_q - v_{cq} - r \times i_{fq} - L \times \omega \times i_{fd} = \frac{L}{\Omega}\frac{di_{fq}}{dt} \tag{2.4}$$

As can be seen in equations (2.3) y (2.4) there is a cross term, ($\pm L \times \omega \times i_{fd/q}$), that appears in the equations of both axes and prevents obtaining a plant that relates the current in the converter i_f to the voltage in the converter *e*. Therefore, in order to facilitate control, auxiliary variables, $\widehat{e_d}$ y $\widehat{e_q}$ whose equations are as follows:

$$\widehat{e_d} = e_d - v_{cd} + L \times \omega \times i_{fq} \tag{2.5}$$

$$\widehat{e_q} = e_q - v_{cq} - L \times \omega \times i_{fd} \tag{2.6}$$

Substituting (2.5) and (2.6) in (2.3) and (2.4) respectively, we obtain the following equations that allow us to find a common plant for both axes having as command $\widehat{e_d}$ and $\widehat{e_q}$ and as output i_{fd} and i_{fq}. We can subsequently undo the change of variable obtaining the real voltage commands of the converter which are e_d and e_q.

$$\widehat{e_d} = \frac{L}{\Omega}\frac{di_{fd}}{dt} + r \times i_{fd} \tag{2.7}$$

$$\widehat{e_q} = \frac{L}{\Omega}\frac{di_{fq}}{dt} + r \times i_{fq} \tag{2.8}$$

Obtaining a common plant $P_i(s)$, for the current control of both d and q axes:

$$Pi(s) = \frac{1}{r + \frac{L}{\Omega} \cdot s}$$

This plant is used together with a PI control in the Laplace domain to find a second order transfer function to select the correct control parameters, but this is not the purpose of this project. So, we will use a model with some PI control parameters previously studied that work properly.

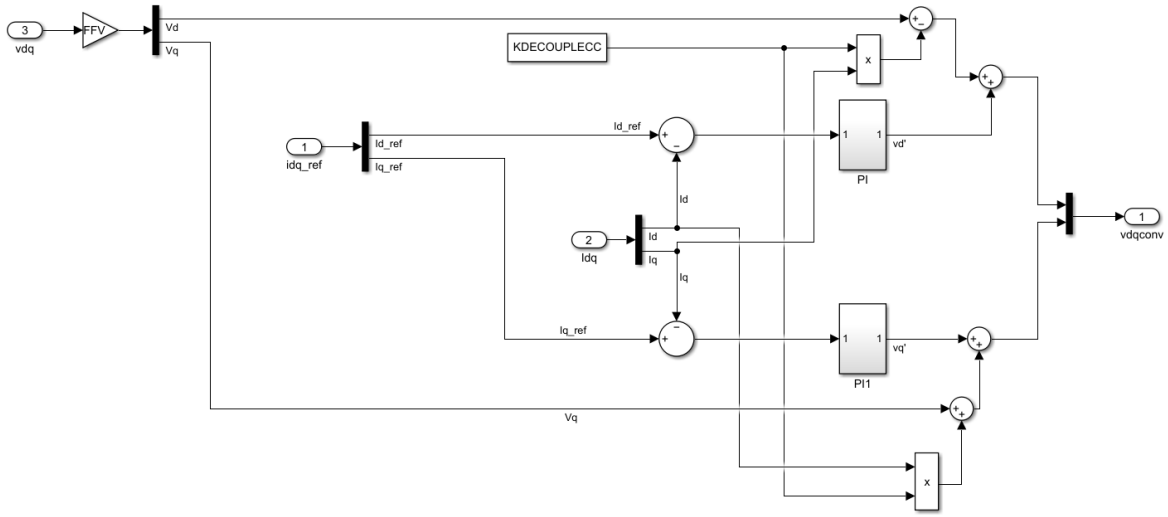

Figure 2.3: Grid forming current control loop of the Simulink Model

Figure 2.3 shows the current control used in the converter model. This control follows the equations explained above. In the model v_{dq} corresponds to v_{cdq}, idq corresponds to i_{fdq}, v_{dq}' to $\hat{e}_{dq}$ and KDECOUPLECC = $\omega \times L$.

2.3.2 IMPLEMENTATION OF OUTER VOLTAGE LOOP

To implement the external voltage loop, the differential equations on dq axes obtained by performing the Clarke-Park transform to equation (2.2) are used.

The equations obtained on dq axes in pu are as follows:

$$i_{fd} - i_{od} + C \times \omega \times v_{cq} = \frac{C}{\Omega}\frac{dv_{cd}}{dt} \tag{2.9}$$

$$i_{fq} - i_{oq} - C \times \omega \times v_{cd} = \frac{C}{\Omega}\frac{dv_{cq}}{dt} \tag{2.10}$$

As can be seen in (2.9) and (2.10) there is a cross term ($\pm C \times \omega \times v_{cd/q}$) that appears in the equations of both axes and prevents from obtaining a plant that relates the capacitor voltage v_c to the converter current i_f directly. Therefore, as in the current control, auxiliary variables $\widehat{i_d}$ and $\widehat{i_q}$ whose equations are:

$$\widehat{i_d} = i_{fd} - i_{od} + C \times \omega \times v_{cq} \tag{2.11}$$

$$\widehat{i_q} = i_{fd} - i_{od} + C \times \omega \times v_{cq} \tag{2.12}$$

Substituting (2.11) and (2.12) in (2.9) and (2.10) respectively we obtain the following equations that allow us to find a common plant for both axes that have as command $\widehat{i_d}$ and $\widehat{i_q}$ and as output v_{cd} and v_{cq}. Being able later to undo the change of variable obtaining the real current commands of the converter which are i_{fd} and i_{fq} that will be the current references for the internal current loop.

$$\widehat{i_d} = \frac{C}{\Omega}\frac{dv_{cd}}{dt} \tag{2.13}$$

$$\widehat{i_q} = \frac{C}{\Omega}\frac{dv_{cq}}{dt} \tag{2.14}$$

Obtaining a common plant $P_v(s)$, for the voltage control of both d and q axes:

$$Pv(s) = \frac{\Omega}{C \cdot s}$$

In the model this plant is only used for the design of the control parameters. In the case of our model, which already has designed parameters, the capacitor voltage is taken as a measurement and the voltage reference obtained from the reactive power loop is followed.

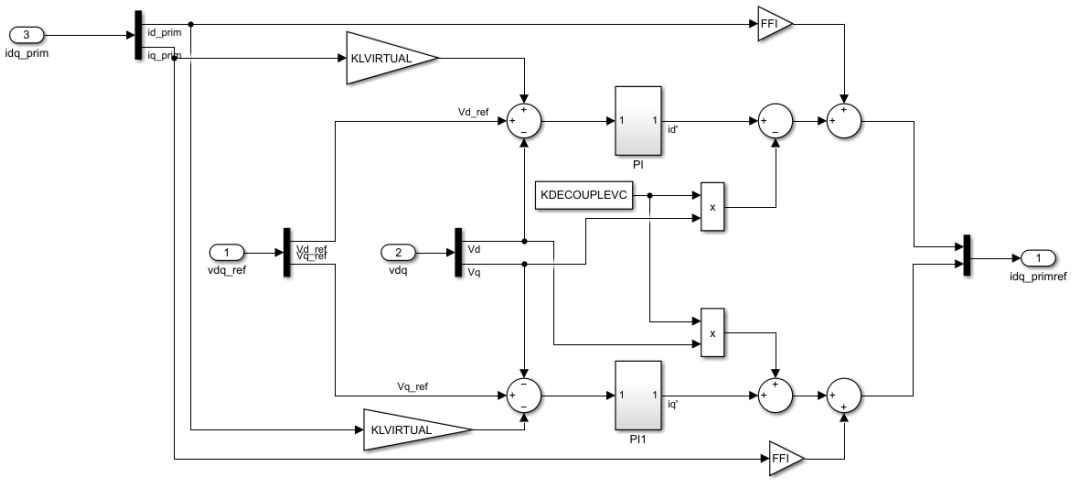

Figure 2.4: Grid forming voltage control loop of the Simulink Model

Figure 2.4 shows the voltage outer loop implemented in the Simulink model following the equations shown above. In the model v_{dq} corresponds to v_{cdq}, i_{dq_prim} corresponds to i_{fdq}, i_{dq}' to $\hat{\imath}_{dq}$ and KDECOUPLEVC = $\omega \times C$.

2.4 POWER CONTROL LOOPS

The power loop is divided into two parts, the active power loop and the reactive power loop. To give a generic view, the active power loop is in charge of the primary regulation, the setting of the frequency of the converter and the contribution of the synthetic inertia of the converter to the grid, which is the object of study of this project. While the reactive power loop is responsible for generating a reference voltage of the capacitor for the voltage control, to set the desired voltage in the grid.

In this project two different active power control designs have been studied, the frequency droop control and the VSM type control whose equivalence and characteristics are explained in detail in *section 2.4.*

The reactive power loop is based on the voltage droop method, whose behavior is very similar to the frequency droop and is explained in *section 2.4.1*.

In order to understand the principle of operation of voltage and frequency droop control it is first necessary to understand the flow of active and reactive power between two voltage phasors separated by an impedance. This is really the basic principle of operation of primary regulation. In the case of the microgrid under study here, the voltage phasors would be those corresponding to the converter node and the capacitor node, and the impedance would be the one of the filter, which can be represented as a single inductance. Thus, leaving a simplified scheme as shown in Figure 2.5.

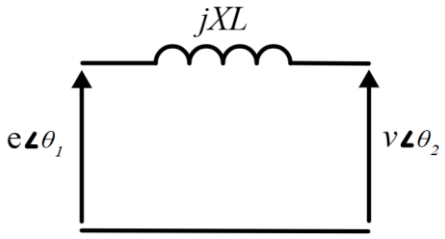

Figure 2.5: single-line diagram of two voltage phasors separated by an inductance.

Therefore, if it is assumed that the resistance in the line is negligible compared to the transformer inductance $z = j \cdot xL$. And the equation $\bar{s} = p + jq = \bar{e} * \overline{(i)}^*$ is developed, expressing the current in terms of the voltage difference and the impedance we arrive at the following equations in pu which represent the power flow from the voltage phasor $\bar{e}$ of the converter to the voltage phasor $\bar{v}$ of the capacitor:

$$p = \frac{e * v * \sin(\theta_1 - \theta_2)}{X} \tag{2.15}$$

$$q = \frac{e * (e - \mathrm{v} * \cos(\theta_1 - \theta_2))}{X} \tag{2.16}$$

$$\delta = \theta_1 - \theta_2 \tag{2.17}$$

If the grid is operating under standard conditions, the angle in (2.16) should be small and the voltage at the capacitor constant, however, in equations [(2.18) - (2.23)] both the approximation and the exact equation are included since in this project the converter will be studied under normal and current limit conditions and the exact expressions will be necessary to understand the behavior of the converter.

$$\frac{\partial p}{\partial e} = \frac{v * \sin(\delta)}{X} \approx 0 \tag{2.18}$$

$$\frac{\partial p}{\partial v} = \frac{e * \sin(\delta)}{X} \approx 0 \tag{2.19}$$

$$\frac{\partial p}{\partial \delta} = \frac{e * v * \cos(\delta)}{x} \approx \frac{e * v}{x} \tag{2.20}$$

$$\frac{\partial q}{\partial e} = \frac{2 * e - v * \cos(\delta)}{x} \approx \frac{2 * e - v}{x} \tag{2.21}$$

$$\frac{\partial q}{\partial v} = \frac{-v * \cos(\delta)}{x} \tag{2.22}$$

$$\frac{\partial q}{\partial \delta} = -\frac{e * v * \sin(\delta)}{x} \approx 0 \tag{2.23}$$

Equations [(2.18) - (2.23)] allow us to have an intuition of the operation of the primary regulation of the converter since by varying the angle δ and the modulus of the converter voltage we can modify the active and reactive power delivered to the grid.

Based on this idea it can be seen that transient variations between the capacitor voltage phasor frequency and the converter voltage phasor frequency, which translate into variations of the angle δ, causes the delivered active power to vary following the equation (2.20). Similarly, variations in the converter voltage modulus causes variations in the reactive power delivered to the grid following the equation (2.21). Hence the terms frequency droop and voltage droop.

2.4.1 DROOP CONTROL

The droop control is based on the idea of emulating the droop characteristic of synchronous generators in power electronics. For this purpose, the controls are implemented based on equations (2.24) and (2.25), which correspond to the frequency and voltage droop respectively in the time domain. Although to implement the controls we will use equations (2.26) and (2.27) in the Laplace domain.

$$\omega(t) = \omega^* + (p^* - p(t)) \cdot \frac{1}{D_{Pdroop}} \tag{2.24}$$

$$v(t) = v^* + (q^* - q(t)) \cdot \frac{1}{D_{Qdroop}} \tag{2.25}$$

$$\omega = \omega^* + m_p \cdot (p^* - p) \cdot \frac{1}{1 + T_{Pdroop} \cdot s} \tag{2.26}$$

$$v_{dref} = 1 + m_q \cdot (q^* - q) \cdot \frac{1}{1 + T_{Qdroop} \cdot s} \tag{2.27}$$

In equation (2.24):

- $\omega(t)$ is the frequency of the converter.
- ω^* is the frequency setpoint, which in the case of the converter under study is constant ($\omega^* = 1\ pu$).

- D_{Pdroop} is the frequency droop constant and is equivalent to the inverse of the droop in a synchronous machine, i.e., $D_{Pdroop} = \frac{1}{m_p}$.
- $p(t)$ is the active power delivered to the network by the converter.
- p^* is the reference power that in the case of our converter, which only participates in the primary regulation, is a constant with value the active power obtained as a result of calculating the system load flow.

In equation (2.26) all the variables are analogous to those in equation (2.24) but in the Laplace domain. The only new constant is T_{Pdroop}, which is the time constant of the low pass filter.

In equation (2.25):

- $v(t)$ is the capacitor voltage.
- v^* is the voltage set point, which in the case of the model used, is $v^* = 1\ pu$.
- D_{Qdroop} is the voltage droop constant and is also $D_{Qdroop} = \frac{1}{m_q}$.
- $q(t)$ is the reactive power delivered to the grid by the converter.
- q^* is the reference power that in the case of our converter that only participates in the primary regulation is a constant with value the reactive power obtained as a result of calculating the system load flow.

In equation (2.27), the variables are analogous to those of equation (2.25) in the Laplace domain. The only notable differences are the time constant T_{Qdroop} of the filter and that the capacitor voltage is on dq axes. As explained in *section 2.2* we are going to work on dq axes to be able to control the variables. In addition, for ease of control one of the two components of the voltage control reference voltage is made zero. It can be either the d or the q component so that we only work with the capacitor voltage modulus. In the case of the model studied here, it is the q component of the reference voltage that is made zero.

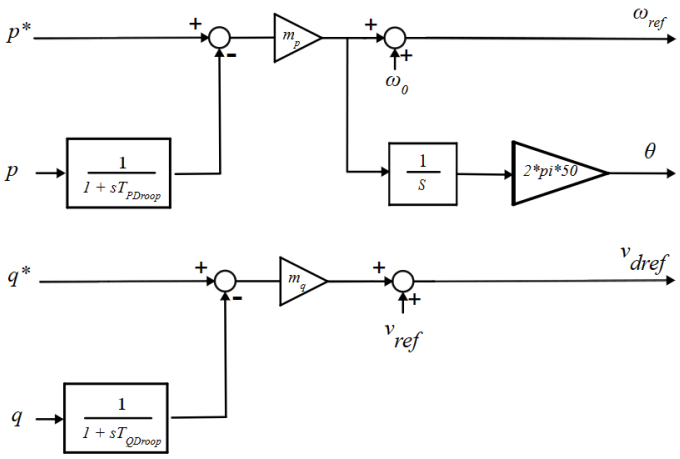

Figure 2.6: Schematic of frequency and voltage droop controls.

Figure 2.6 shows a schematic of the way in which the frequency and voltage droop controls have been implemented in the Simulink model used. The function of the filter incorporated in the equations and also shown in the schematic is, in theory, to damp the oscillations coming from the power measurement, although we will see later that this filter is the origin of the inertial behavior of the droop control and also of the equivalent VSM model as explained in *section 2.4.3*.

The angle θ obtained as the integral of the frequency deviation of the converter is the one used as Park's theta to make the conversion to dq-axes and also represents the deviation of the angle δ seen in equations [(2.18) - (2.23)]. So that when there is an instantaneous power unbalance in the network as a consequence of the loss of a generation, this angle updates the voltage and current values in dq axes, which in turn update the active and reactive power delivered to the network in dq axes according to the equations:

$$p = v_d * i_d + v_q * i_q \tag{2.28}$$

$$q = v_q * i_d - v_d * i_q \tag{2.29}$$

2.4.2 VSM CONTROL

VSM (Virtual Synchronous Machine) control is based on numerically replicating the model of a synchronous machine. In the literature you can find different ways to implement VSM control depending on the complexity with which you want to emulate the synchronous generator. The simplest model, which is the one to be treated in this study, is based on the swing equation defined in (2.30) in the time domain and in (2.31) in the Laplace domain. It will be the latter equation that will be used to implement the control in the model. Both equations are defined in pu with respect to the power and frequency bases of the converter.

$$2H \cdot \frac{d\omega}{dt} = p_m - p_e - D_{SM}(\omega - 1) \tag{2.30}$$

$$\Delta\omega(s) = \frac{\Delta p_m(s) - \Delta p_e(s)}{2 \cdot H \cdot s + D_{SM}} \tag{2.31}$$

In equation (2.30):

- ω is the rotor frequency in pu.
- p_m and p_e are the mechanical and electrical power in pu respectively.
- D_{SM} is the damping factor of the synchronous machine.
- $2H$ represents the inertia constant of the machine.

It should be noted as developed in [10] that both D_{SM} and $2H$ are frequency dependent and can only be considered constant for small changes in frequency.

Equation (2.31) defines the Laplace transform of equation (2.30) for small variations of frequency and power. Developing this equation, equation (2.32) is obtained.

$$2 \cdot H_{vsm} \cdot s.\, \omega_{vsm} = p^* - p_e - D_{VSM} \cdot (\omega_{vsm} - \omega^*) \tag{2.32}$$

In equation (2.32):

- ω_{vsm} and ω^* are the virtual frequency of the converter and the grid frequency respectively.
- p^* and p_e are the reference power, obtained from performing the system load flow and the electrical power delivered by the converter respectively.
- D_{VSM} is the virtual damping factor of the VSM represents in a simplified way the effects of the damping windings of the real synchronous machine. Furthermore, $D_{VSM} = \frac{1}{M_{Pvsm}}$ where M_{Pvsm} is the virtual droop constant.
- $2H_{vsm}$ is the synthetic inertia constant of the VSM.

Figure 2.7 shows the control scheme used to implement VSM control.

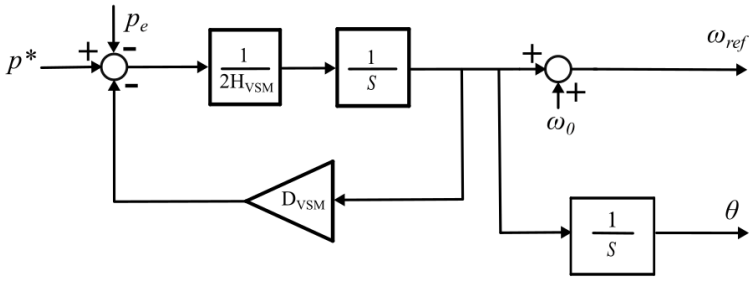

Figure 2.7: VSM control scheme.

By applying basic block algebra techniques to the control scheme in Figure 2.7 we can obtain the transfer function shown in Figure 2.8.

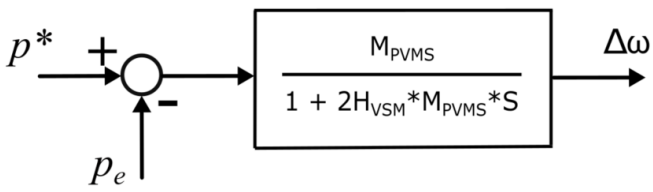

Figure 2.8: Equivalent transfer function of VSM control

As we can see the implementation of the VSM control simply consists of a low pass filter in which the filter time constant depends on the inertia constant $2H_{vsm}$ and the droop constant M_{Pvsm}. This deduction serves as an introduction to the next section in which the equivalence of the two power controls studied under certain conditions as done in [5] is going to be emphasized.

2.4.3 DROOP AND VSM EQUIVALENCE

As mentioned in other sections, it is possible to find an equivalence between the simplified *vsm* control based on Newton's second law of rotation, and the *droop* control explained in *section 2.4.1*.

This equivalence is given if the power reference p^* is constant and if the frequency setpoint ω^* is constant, conditions that are met in this case since the reference power of the converter comes from calculating the power delivered to the grid from the result of the load flow and the frequency setpoint being a Grid Forming converter without PLL is $\omega^* = 1\ pu$.

Therefore, if we develop the equation coming from the droop control scheme seen in Figure 2.6 where p_e is the power at the output of the filter, we obtain the following equation:

$$p_e = \left(1 + T_{Pdroop} \cdot s\right) \cdot \left(\frac{1}{m_p}(\omega^* - \omega) + p^*\right) \tag{2.33}$$

Operating equation (2.33) and taking into account that the terms $s \cdot p^*$ and $s \cdot \omega^*$ are null because they are the derivative of constant parameters in the Laplace domain, we arrive at the expression (2.34).

In which if we take into account (2.35) and (2.36) the resulting equation is the same as that of the vsm mentioned in (2.32).

$$T_{Pdroop} \cdot \frac{1}{m_p} \cdot s \cdot \omega = p^* - p_e - \frac{1}{m_p}(\omega - \omega^*) \tag{2.34}$$

$$2 \cdot H_{vsm} = T_{Pdroop} \cdot \frac{1}{m_p} \tag{2.35}$$

$$D_{VSM} = \frac{1}{m_p} \tag{2.36}$$

2.4.4 CHOICE OF VSM PARAMETERS

To choose the appropriate M_{Pvsm} droop constant of the grid forming converter, what is usually done is a small signal analysis using the linearized model of the whole system so that the linear system is stable and then it is verified with simulations for different conditions on the nonlinear system that these parameters do not cause instability in the system.

Due to the complexity of this method and the fact that this study is beyond the scope of this project, a classical method seen in [11] has been used instead, which consists of establishing a maximum steady-state frequency variation as a small percentage of the nominal frequency when a step in power equal to 1 pu occurs. Theoretically an acceptable percentage of frequency variation in the network is 5% of the nominal frequency, although it depends on the type of network involved.

Therefore, knowing that the definition of droop follows the expression seen in (2.36), it has been simulated for different scenarios the operation of the network before and after the failure for a range of M_{Pvsm} values ranging from 0.01 pu to 0.05 pu, which means a maximum frequency variation ranging from 1% to 5%.

It has been concluded that for a range of values from 0.01 to 0.03 the grid is stable and the higher the value of droop the more the grid tends to become unstable for high inertia values.

As the value of M_{Pvsm} is normally chosen in order to distribute the contribution to the primary regulation among the different converters of the system, and the value chosen must be such

as to allow the stability of the system, in this project a droop constant M_{Pvsm} = 0.01 pu has been chosen for the study of the impact of inertia.

The value of the virtual inertia constant also influences the stability of the network as it influences the response time of the converter to a variation in power. If we increase the inertia constant too much, the response can be very slow and in case of small perturbations in the power of the network the control can act out of phase so that it increases the oscillations in the network making the system unstable.

For this reason, the tests will be performed for a range of values of the inertia constant ranging from H_{VSM} = 1 pu to H_{VSM} = 14 pu, which have proven to be stable for our system.

2.5 IMPLEMENTATION IN MATLAB/SIMULINK

2.5.1 Microgrid

In order to study the inertial behavior of the converter under different scenarios, the microgrid model shown in Figure 2.9 has been used.

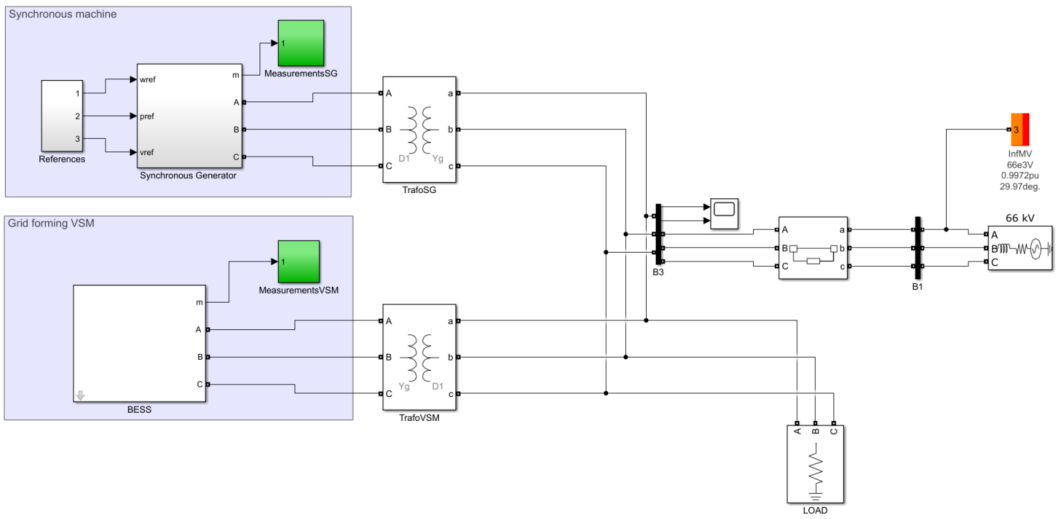

Figure 2.9: Model of the microgrid system implemented in Simulink.

The microgrid operates at 50 HZ and consists of the following elements:

- Synchronous Generator (Sn = 25 MVA, Vn = 6 KV).
- BESS (Battery Energy Storage System) connected through a Grid Forming converter with VSM control to the grid (Sn = 25 MVA, Vn = 400 V).
- Two transformers connecting the above mentioned generating sets to the high side of the grid. The synchronous generator transformer (Sn = 30 MVA, V1/V2 = 66 KV / 6 KV) and the converter transformer (Sn = 30 MVA, V1/V2 = 66 KV / 400 V).
- A purely resistive load whose P_{LOAD} value will depend on the scenario being simulated.

- A switch that separates the three-phase voltage source from the rest of the network and allows simulating the fault at a given instant.
- A three-phase voltage source defined as a PQ node in the network and that will allow us to define the power step we want to simulate, to study the response of the converter.

The operating conditions for each scenario will be explained in *chapter 3*, since in this figure only one of the scenarios has been presented in order to give a clearer view of the system. The real model used includes another synchronous generator that allows simulating the different scenarios.

2.5.2 Inverter

This section presents the converter block to give an overview of its subsystems and how it has been implemented in Simulink.

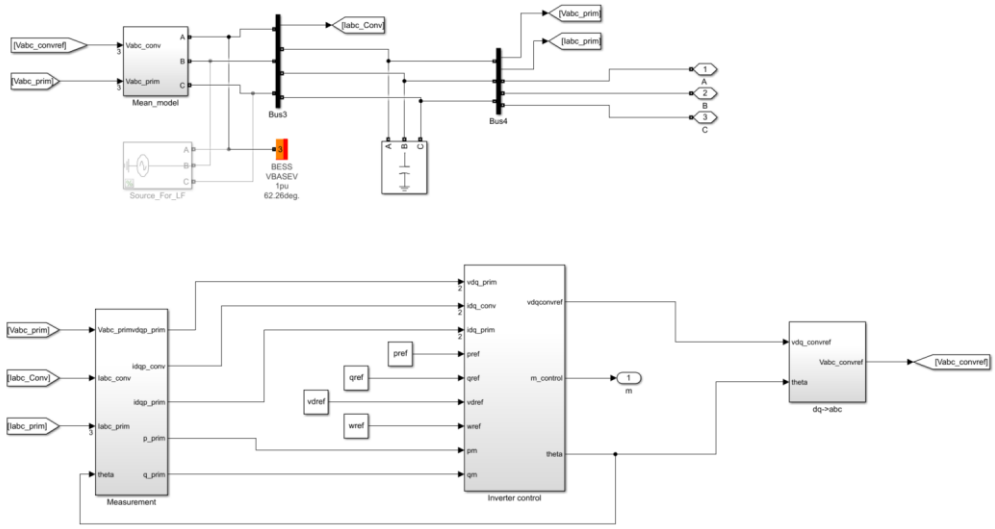

Figure 2.10: Model of the Grid Forming converter implemented in Simulink.

Figure 2.10 shows at the top the VSC converter, the LC filter needed to remove harmonics and the connections to the three-phase grid. In this case, the transistors have been replaced

by a three-phase ideal current source whose value is calculated from the capacitor voltage measurement and the converter reference voltage obtained from the inverter control. All this together with the RL Branch of the filter is implemented inside the “Mean_model” block.

On the other hand, the lower part of Figure 2.10 is entirely dedicated to the converter control where three blocks can be distinguished:

- The "Measurement" block: the function of this block is to take the three-phase capacitor voltage measurement and the current measurements from the grid and the converter, make the park transform and generate from them the power measurements in dq axes used in the control according to equations (2.28) and (2.29).
- The "Inverter Control" block includes the power loop, and the cascade voltage and current control and its objective is to generate the reference voltage of the converter from the measurements on dq axes. Since the study of the project revolves around this block, it will be discussed in detail in *subsection 2.5.2.1.*
- The "dq-abc" block simply makes the inverse of the Park transform.

2.5.2.1 Inverter Control

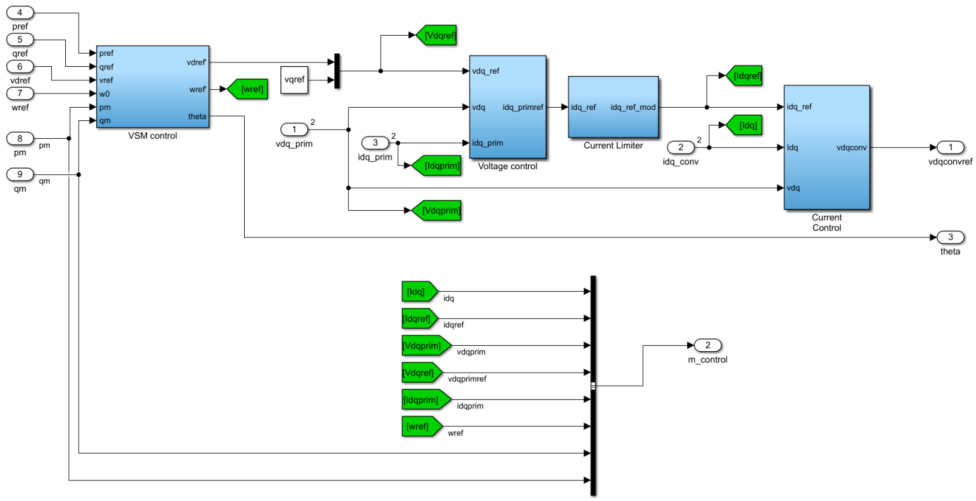

Figure 2.11: Inverter control model implemented in Simulink.

In Figure 2.11 we can see that the inverter control has a power loop, an external voltage loop and an internal current loop as explained in *sections 2.3 and 2.4*. In addition, the control has the "Current_limiter" block whose only function is to establish a limit for the inverter current that allows us to study the inertial response of the converter when the transistors saturate.

The most important block within the control and which has been the object of study and design of this project is the "VSM control" block, whose design is shown in Figure 2.12. In this figure the active and reactive power loops can be observed.

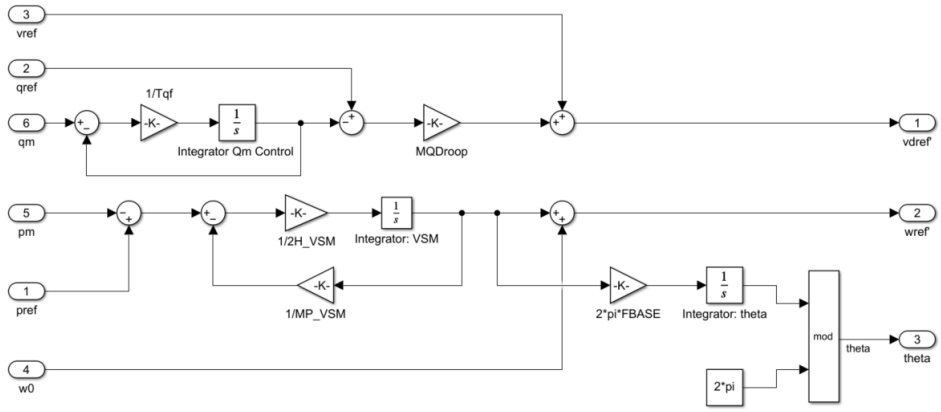

Figure 2.12: VSM Control developed in Simulink.

As explained in section 2.4, the reactive power loop is implemented with a voltage droop control and the active power loop can be implemented as a frequency droop or VSM control.

In regard to the reactive power loop:

- q_m is the reactive power measured at the output of the capacitor in pu, it is followed by a low pass filter with time constant T_{qf} which allows to damp the oscillations coming from the measurement.

- q_{ref} is the reference reactive power in pu, it is constant and is initialized to the reactive power value delivered to the grid according to the results of the load flow.
- M_{QDroop} is the inverse of the voltage droop constant D_{QDroop}.
- V_{ref} is the voltage setpoint at the capacitor and is set to 1 pu.
- V_{dref}' is the "d" component of the capacitor voltage control setpoint in pu.

In regard to the active power loop (VSM):

- p_m is the active power measured at the capacitor output in pu.
- p_{ref} is the reference active power in pu, it is constant and is initialized to the active power value delivered to the network according to the load flow results.
- The control loop that follows has as input the signal (p_{ref} - p_m) and as output $\Delta\omega$. This loop implements the virtual synchronous machine equation described in (2.31), taking into account the equality (2.35).
- ω_0 is the setpoint frequency in pu, it is a constant value in the case where there is no PLL. In this case $\omega_0 = 1\ pu$.
- $\omega_{ref}{}'$ is the virtual frequency of the converter in pu which arises as a result of adding the setpoint frequency and the frequency deviation. In this case it does not have a function as such in the control, it is used only as a measure because we assume $\omega_{ref}{}'$ constant and equal to 1 pu when implementing the voltage and current control. Usually in the literature the frequency $\omega_{ref}{}'$ is integrated to obtain the theta park angle, in this case it has been decided to integrate the frequency deviation $\Delta\omega$ the result is identical if the integrators are correctly initialized in both cases.

2.5.3 Matlab Code

As will be explained in the results, different grid scenarios will be simulated and compared in which there will be different configurations of machines and converters. In addition, for each scenario we intend to study the behavior when certain parameters are varied, such as the inertia constant, the droop of the converters and generators, the magnitude of the power step or the power demanded by the load. To speed up and automate the process, a MATLAB code has been generated, which for each scenario and for desired parameter vectors performs loop simulations and generates the desired plots of the measurements of each scenario against different cases of inertia constant. Figure 2.13 shows a flowchart of the code operation.

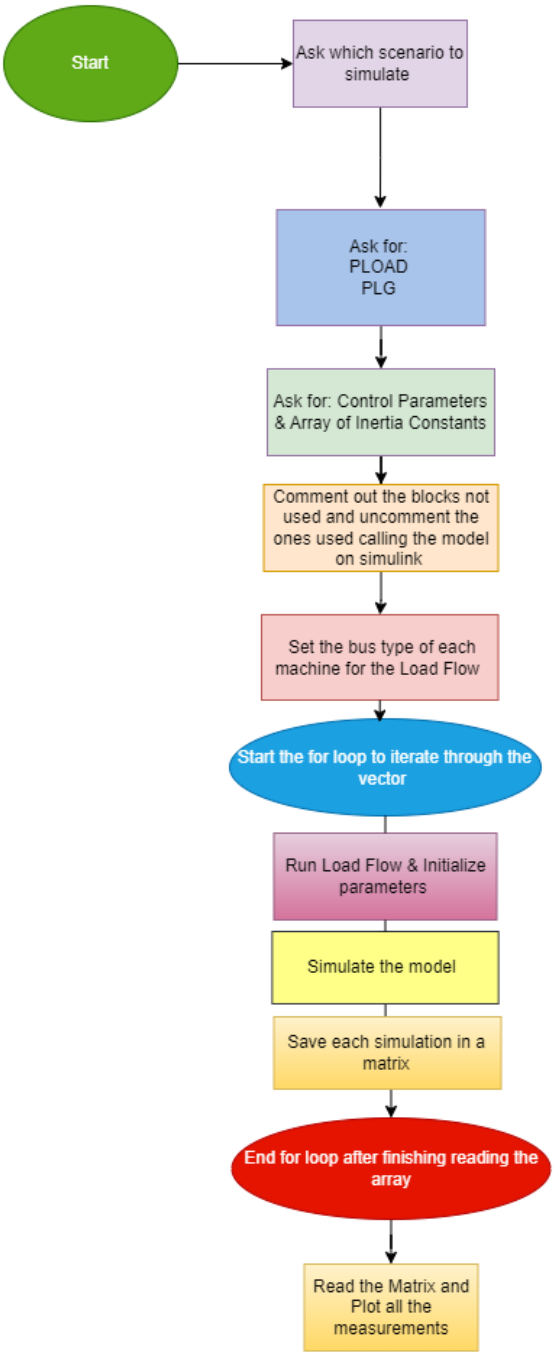

Figure 2.13: Flowchart of Matlab code developed.

Chapter 3. RESULTS

3.1 SYSTEM DESCRIPTION AND CONFIGURATIONS

In order to study the inertial behavior of the converter, different load, inertia constant and droop scenarios of the synchronous machines and the converter will be simulated for three different grid configurations which are explained in detail in the following sections. All configurations have in common the high-voltage side of the grid, which operates at 66 KV and consists of a generator that is lost at a given instant and a purely resistive load.

In addition for all configurations and tests, parameters and variables with subscript "VSM" will refer to the converter, all those with subscript "LG" will refer to the generator that is lost in the failure, parameters with subscript "LOAD" will refer to the load, those with subscripts "SG" will refer to the synchronous generator that appears in both *configuration 2* and *configuration 3*, and parameters with subscript "SG1" will refer to the synchronous generator that appears only in *configuration 3* as a substitute for the converter.

- **Configuration 1: Inverter (VSM) feeding the load**

  In this configuration the low-voltage side of the grid consists only of the grid forming converter of rated apparent power Sn = 25 MVA and rated voltage Vn = 400 V. The current limit of the converter is set as Imax = 1.1 pu. The virtual inertia and droop parameters will be defined in the testing section. Figure 3.1 shows the scheme of *configuration 1* implemented in Simulink.

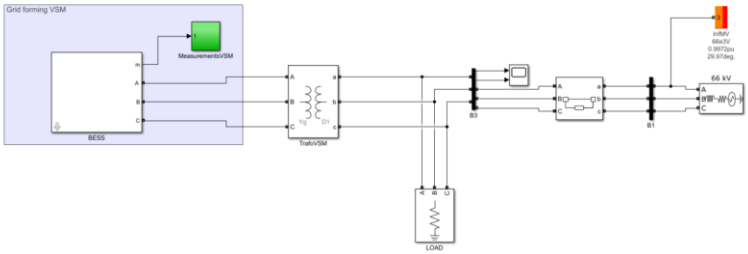

Figure 3.1: Scheme of Configuration 1 implemented in Simulink.

- **Configuration 2: Inverter (VSM) and Synchronous Generator feeding the load**

  In this configuration the low-voltage side of the grid consists of a grid forming converter with VSM control and a synchronous generator with inertia H_{SG} = 6.175 s, and droop M_{SG} = 0.05 pu. The schematic of this configuration has been used as a basis to explain the system used in *section 2.5.1* and is shown in Figure 2.9. The value of the inertia and droop constants of the converter will be defined for each case in the testing section.

- **Configuration 3: Two Synchronous Generators feeding the load**

  This configuration consists of two synchronous generators. The first one is the same as in *configuration 2* with inertia H_{SG} = 6.175 s and M_{SG} = 0.05 pu. The second one with different inertia and droop for each test and equal to those of the converter of *configuration 2* in order to compare the behavior of the synchronous machine with that of the converter. Figure 3.2 shows the schematic of *configuration 3*.

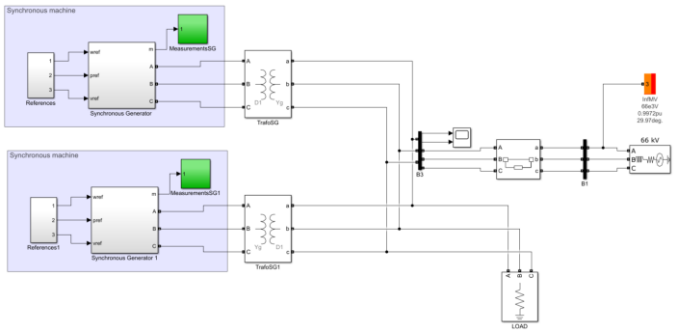

Figure 3.2: Scheme of Configuration 3 implemented in Simulink.

3.2 TESTS

3.2.1 Steady-state frequency and derivative of frequency at t = 0^+

The first test consists of simulating a grid failure under standard conditions for *configuration 2*, i.e., both the converter and the synchronous generator have sufficient reserve to supply the increase in demand. The loss of a generator providing an active power, PLG, is going to be simulated. The value of this constant and the value of the active power demand, PLOAD, are chosen in such a way that for each of the configurations no current limits are reached in case of the converter. The purpose of this test is to verify the correct operation of the system by checking that the simulations comply with the theoretical calculations of the steady state frequency and the derivative of the frequency at the initial instant according to equations (3.1) and (3.2) respectively.

$$\Delta f_{ss} = \frac{\Delta p}{\frac{1}{m_{vsm}} + \frac{1}{m_{SG}}} \tag{3.1}$$

$$\left.\frac{df_{COI}}{dt}\right|_{t=0^+} = \frac{\Delta p}{2 \cdot \sum_i H_i} \tag{3.2}$$

Table 3-1 presents the parameters chosen to achieve the operating conditions explained above.

Δp	M_{PVSM}	H_{VSM}	M_{SG}	H_{SG}	S_{BSG}	S_{BVSM}
0.4 pu	0.01 pu	1 s	0.05 pu	6.175 s	25 MVA	25 MVA

Table 3-1: Parameters of the grid used for test 1.

The frequency of the converter and generator must converge in steady state to the value $f_n + \Delta f_{ss}$. Substituting the values from Table 3-1 into equation (3.1) gives that theoretically $\Delta f_{ss} = -\frac{0.4}{\frac{1}{0.01}+\frac{1}{0.05}} = -3.33 * 10^{-3}$ pu.

On the other hand, using equation (3.2) and substituting the values in the table, we obtain that $\frac{df}{dt}_{t=0^+} = \frac{0.4}{2*(6.175+1)} = 2.79 * 10^{-2}$ pu.

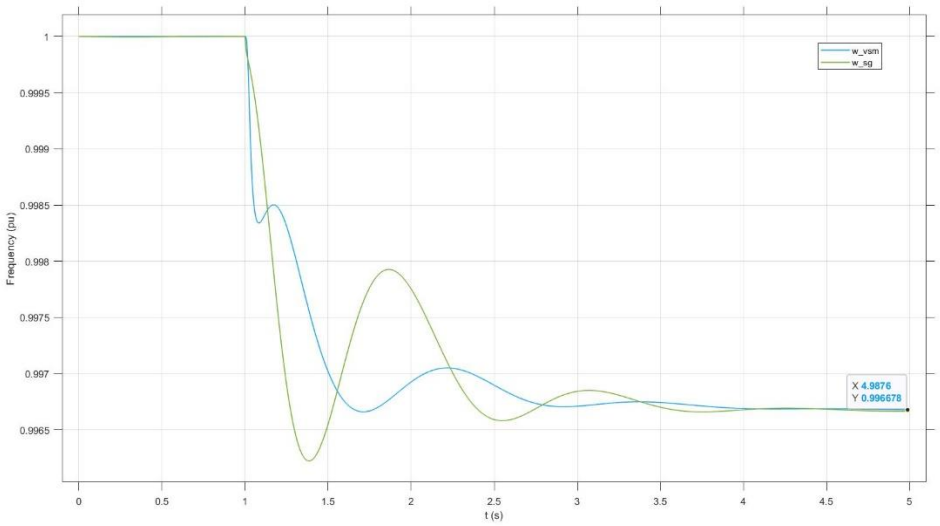

Figure 3.3: Frequency of VSM and SG.

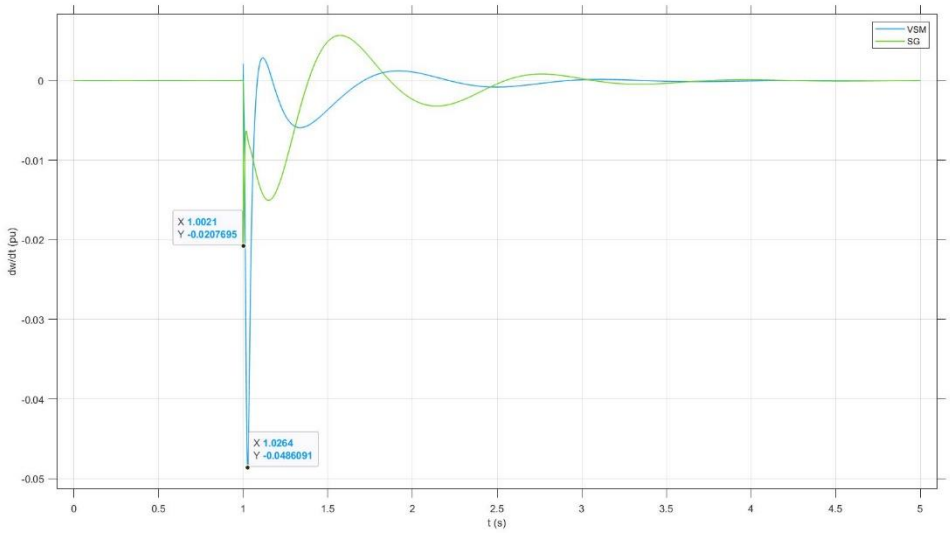

Figure 3.4: Derivative of SG and VSM frequency.

Figure 3.3 shows the simulated frequency of both the synchronous machine and the converter. The behavior at first glance is as expected since at the instant of failure the frequency drops causing a transient in both machines that end up converging to the frequency value of the grid in steady state. In the figure it can be seen that $f_{ss} = 0.996678$ and therefore $\Delta f_{ss} = 0.996678 - 1 = -3.32 * 10^{-3}$ pu which coincides with the expected theoretical value.

On the other hand, in Figure 3.4 we can see the derivative of the frequency of the synchronous machine and the converter. The Figure 3.4 also shows the value of the maximum derivative in absolute value, which theoretically coincides with the initial instant since at $t = 0^+$ (considering t = 0 as the instant of failure) the machines are not yet regulating, and the frequency drop is maximum. This has been done in order to calculate $\frac{df}{dt}_{t=0^+}$ and compare it with the expected theoretical value. To obtain the derivative of the grid frequency at the initial instant, a weighted average of the $\frac{df}{dt}_{t=0^+}$ value of each machine must be made according to equation (3.3).

$$\frac{df_{mean}}{dt}_{t=0^+} = \frac{\sum_i \frac{df_i}{dt}_{t=0^+} * H_i}{\sum_i H_i} \quad (3.3)$$

Substituting the value $\frac{df_{SG}}{dt}_{t=0^+} = -0.0207695$ and $\frac{df_{VSM}}{dt}_{t=0^+} = -0.0486091$ obtained from the simulation along with the parameters of the inertia constants from Table 3-1 into equation (3.3), we obtain that $\frac{df_{mean}}{dt}_{t=0^+} = -2.46 * 10^{-2}$ pu. Which implies an error of about 11 % versus theoretically expected. This error can be explained by the fact that the theoretical calculation does not take into account effects such as voltage drop that decrease the power to be delivered by the generator sets and therefore also Δp. To take this into account in theoretical calculations, if we look at Figure 3.13, we can see that the voltage at the initial instant is approximately 0.94 pu. Being a purely resistive load, the power varies quadratically with the voltage. In other words, it would actually be demanding approximately 88% of what it originally demanded. This leads us to the theoretical value of the derivative at the initial instant to be $\frac{df}{dt}_{t=0^+} = \frac{0.4*(0.94)^2}{2*(6.175+1)} = 2.46 * 10^{-2}$ pu, which coincides with the obtained value.

3.2.2 Study of converter inertial response for standard conditions

The purpose of this test is to study the inertial behavior of the converter when there is a failure in the grid under standard conditions. That is to say, the loss of a generator at a given instant will be simulated and the converter and/or the synchronous machine, depending on the configuration, will have enough reserve to supply the demand and none of them will reach its current limit in any case. This test will be performed for different values of converter inertia for each of the configurations. The objective is to study and draw conclusions of the converter behavior for different inertia values when operating on a regular basis in order to later compare its performance under limit conditions.

- **Configuration 1**

In order that the converter does not reach the current limit and has sufficient reserve for primary regulation, the scenario presented in Table 3-2 has been chosen.

Δp	M_{PVSM}	P_{LOAD}	P_{LG}	S_{BVSM}
0.2 pu	0.01 pu	15 MW	5 MW	25 MVA

Table 3-2: Initial parameters used for test 2 - configuration 1.

For this case, the following measurements have been obtained to understand the operation of the synthetic inertia of the converter:

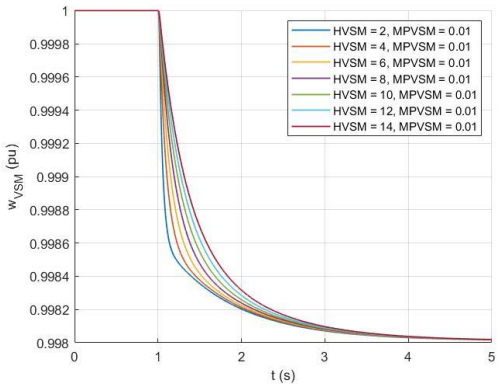

Figure 3.5: Inverter frequency for different inertia values.

Figure 3.5 shows the frequency behavior of the converter with a step in the generation for different values of the virtual inertia of the converter. It can be seen a first order response whose time constant increases proportionally with the H_{VSM} constant. The first order frequency response to a power step causes the nadir frequency to coincide with the steady state frequency as shown numerically in Table 3-4.

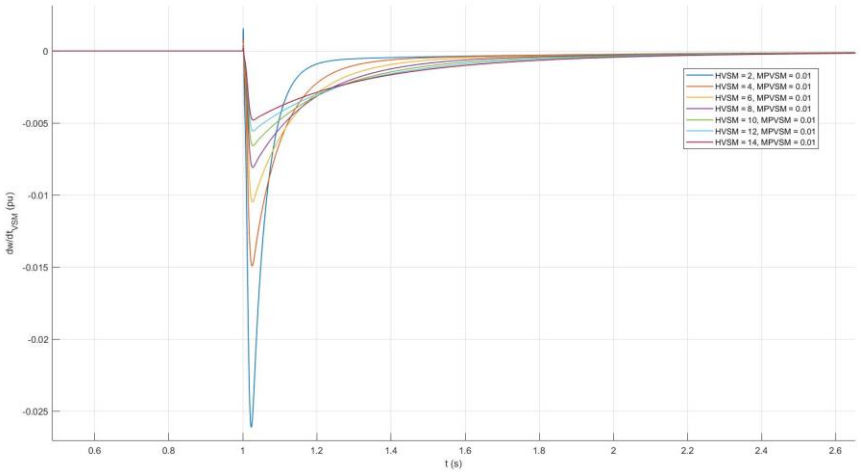

Figure 3.6: Inverter frequency derivative for different inertia values.

Figure 3.6 shows the RoCoF of the inverter and will allow us to highlight one of the differences between the inverter with VSM control and the synchronous machine in terms of inertial response. This difference lies in the fact that the frequency derivative of the inverter at the initial instant is positive, which does not occur in the synchronous machine. The explanation of this difference will be detailed in *section 3.3* once the graphs of the necessary measurements have been presented. In addition, to facilitate the understanding and comparison of the different scenarios, the values of the maximum RoCoF in absolute value for each of the values of the inertia constants are included in Table 3-3. Which show that as the inertia constant increases, the rocof decreases, although not exactly in proportion.

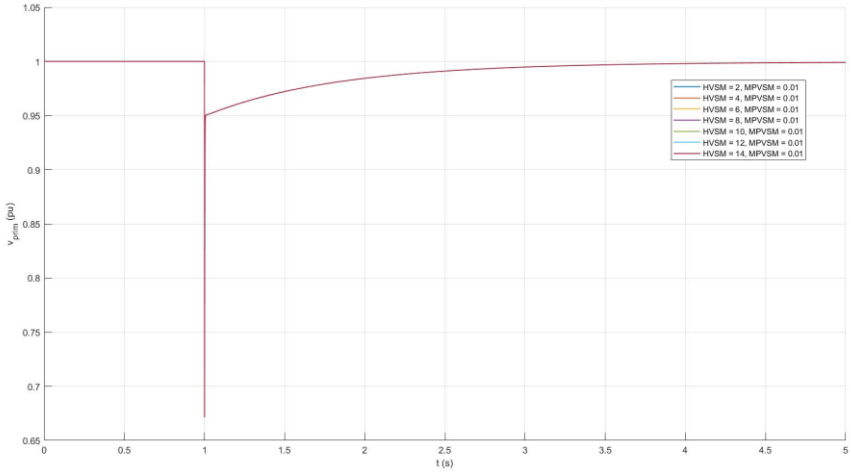

Figure 3.7: Voltage at the capacitor for different inertia values

Figure 3.7 shows the behavior of the capacitor voltage when the inverter operates within its limits. It is able to impose the voltage on the grid and regulate it when the loss occurs, returning it to its original state thanks to the action of the integral control.

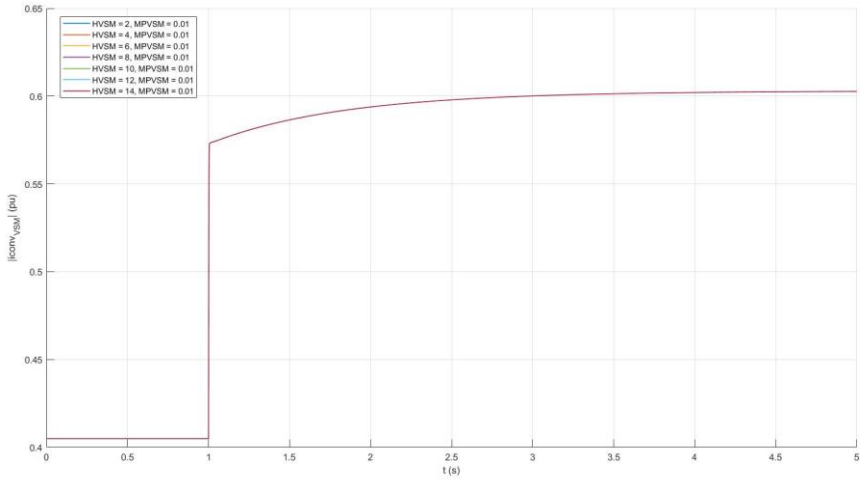

Figure 3.8: Inverter current for different inertia values.

Figure 3.8 is presented in order to demonstrate that the current in the converter does not saturate, i.e., at any moment the maximum allowed current I_{MAX} = 1.1 pu is reached.

The capacitor voltage and the converter current are closely related as will be seen later and will become more relevant in the comparisons section.

H_{VSM} (s)	$\|RoCoF\|_{MAX}$ (pu/s)
2	$26.12*10^{-3}$
4	$14.92*10^{-3}$
6	$10.49*10^{-3}$
8	$8.09*10^{-3}$
10	$6.58*10^{-3}$
12	$5.53*10^{-3}$
14	$4.78*10^{-3}$

Table 3-3: Maximum RoCoF in absolute value.

$Nadir_{VSM}$ (pu)	f_{ss} (pu)
0.996673	0.996673

Table 3-4 : Frequency nadir and steady state frequency

- **Configuration 2**

To achieve a scenario similar to that of *configuration 1*, where the limits of the converter and the synchronous machine are not reached, the parameters and initial conditions shown in Table 3-5 have been selected:

Δp	M_{PVSM}	M_{SG}	H_{SG}	P_{LOAD}	P_{LG}	P_{VSM}	S_{VSM}	S_{BSG}
0.4 pu	0.01 pu	0.05 pu	6.175 s	30 MW	10 MW	10 MW	25 MVA	25 MVA

Table 3-5: Initial parameters used for test 2 - configuration 2.

The following results were obtained for this scenario**:**

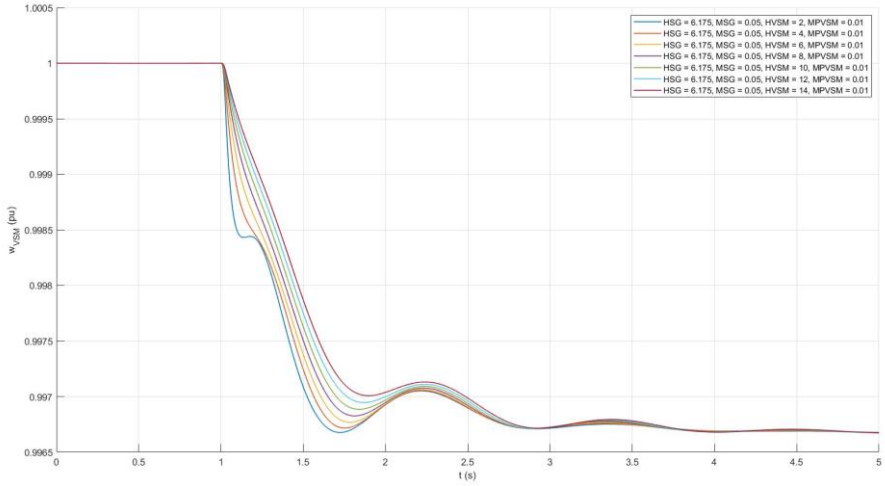

Figure 3.9: VSM frequency for different values of virtual inertia.

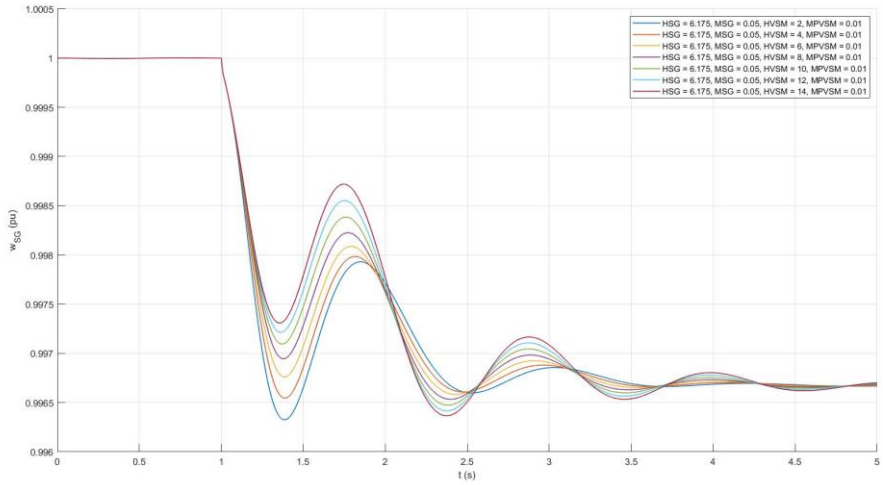

Figure 3.10: SG frequency for different values of virtual inertia.

Figure 3.9 and Figure 3.10 show the frequency behavior of the inverter and synchronous generator respectively. It can be seen, how the inverter frequency no longer looks like the shape of the step response of a first order system. This is due to oscillations resulting from the interaction of the rotor equation (real or synthetic) between the two machines. These oscillations are due to the transient frequency difference between the inverter and the synchronous generator. However, the oscillations are not sufficient to make the nadir frequency of the converter in either case different from the steady-state frequency, as shown numerically in Table 3-7.

Regarding the frequency of the synchronous generator, it is possible to observe that the nadir frequency for the different converter inertias is lower than the steady-state frequency as a consequence of the oscillations superimposed on the over-damped fourth order response of the synchronous machine and steam turbine system implemented in Matlab for the chosen droop and inertia parameters. The values of the nadir frequency for each case are presented in Table 3-6.

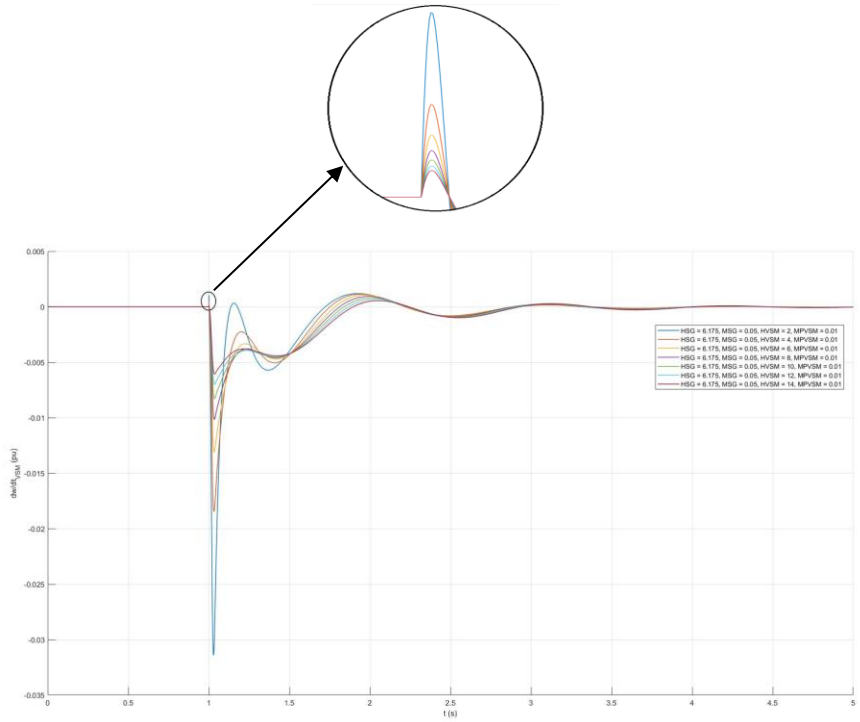

Figure 3.11: Derivative of VSM frequency for different values of virtual inertia.

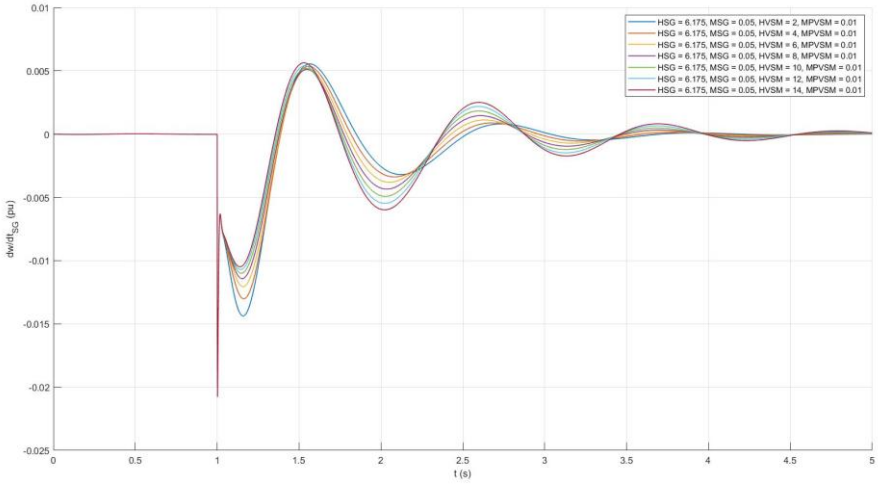

Figure 3.12: Derivative of SG frequency for different values of virtual inertia.

Figure 3.11 and Figure 3.12 present the frequency derivative of the converter and the synchronous generator respectively. In the case of the converter, we can see that the maximum RoCoF in absolute value is higher the lower the frequency. This is confirmed numerically in Table 3-6. In the case of the generator, we can see that the RoCoF at the initial instant is the same for all cases and its value is detailed in Table 3-7.

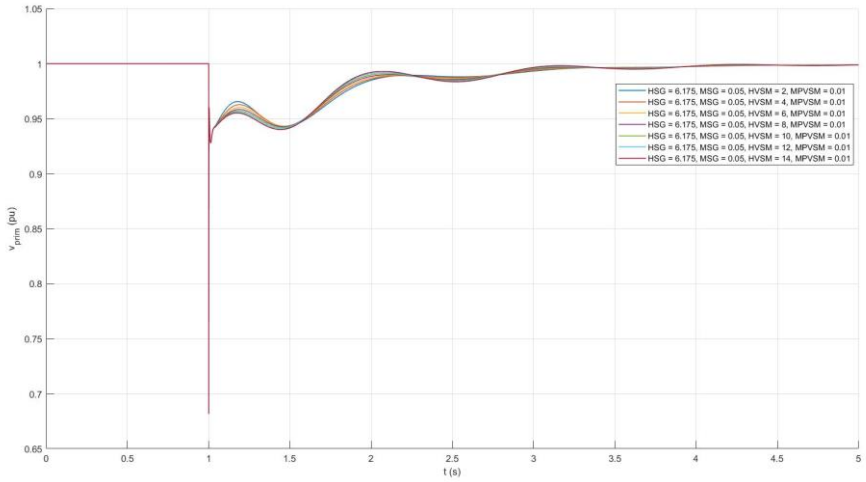

Figure 3.13: Voltage at the capacitor for different values of virtual inertia.

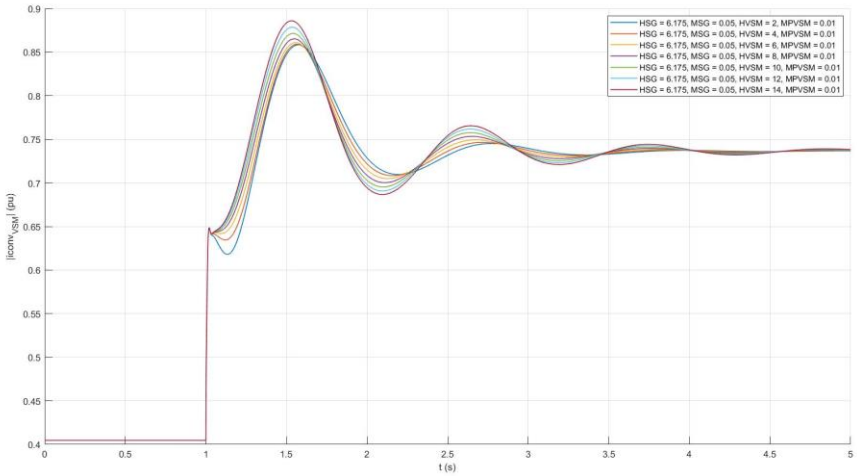

Figure 3.14: Inverter current for different inertia values.

Figure 3.13 and Figure 3.14 show the capacitor voltage and the converter current respectively. It can be seen how both show oscillations as a consequence of the combined action of the machines.

H_{VSM} (s)	$\|RoCoF_{VSM}\|_{MAX}$(pu/s)	$Nadir_{SG}$
2	$31.41*10^{-3}$	0.996327
4	$18.46*10^{-3}$	0.996545
6	$13.10*10^{-3}$	0.996585
8	$10.16*10^{-3}$	0.996535
10	$8.30223*10^{-3}$	0.996475
12	$7*10^{-3}$	0.996416
14	$6.01*10^{-3}$	0.996367

Table 3-6: VSM maximum RoCoF in absolute value and SG nadir frequency.

$\|RoCoF_{SG}\|_{t=1^+}$(pu/s)	$Nadir_{VSM}$ (pu)	f_{ss} (pu)
$20.77*10^{-3}$	0.996673	0.996673

Table 3-7: SG RoCoF at the instant of failure, VSM nadir frequency and steady state frequency.

- **Configuration 3**

  In this case, we simulate exactly the same scenario as in *configuration 2*, but now a synchronous generator acts as the grid forming inverter, which will allow us to study the differences between the converter with VSM control and the synchronous machine. The grid parameters for this scenario can be found in Table 3-8.

Δp	M_{SG1}	M_{SG}	H_{SG}	P_{LOAD}	P_{LG}	P_{SG1}	S_{SG1}	S_{BSG}
0.4 pu	0.01 pu	0.05 pu	6.175 s	30 MW	10 MW	10 MW	25 MVA	25 MVA

Table 3-8: Initial parameters used for test 2 - configuration 3.

The following results have been obtained for this scenario:

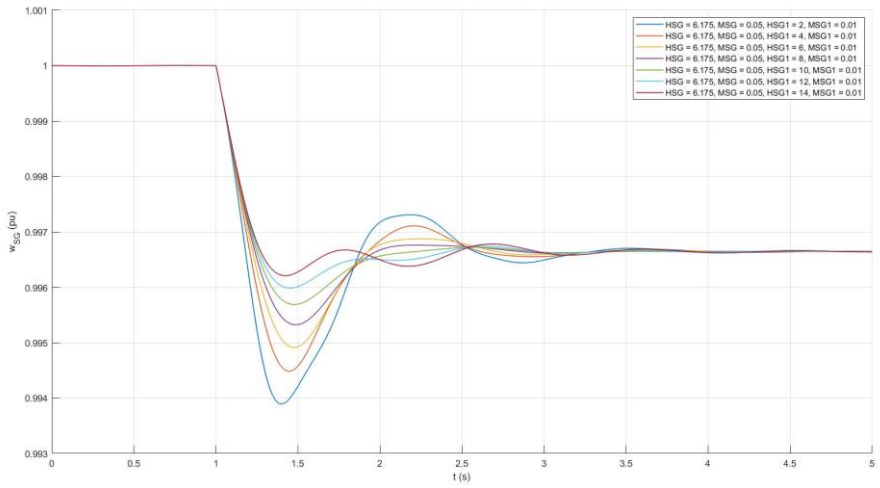

Figure 3.15: SG frequency for different values of virtual inertia.

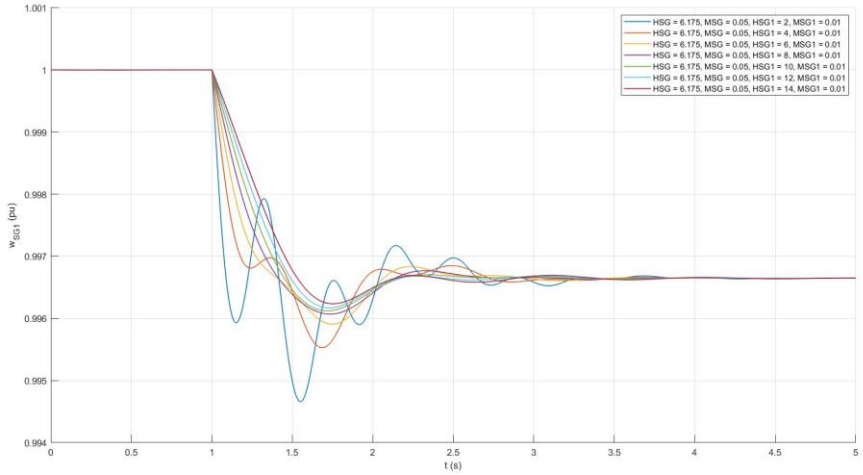

Figure 3.16: SG1 frequency for different values of virtual inertia.

Figure 3.15 and Figure 3.16 show the frequency of both synchronous generators. As shown numerically in Table 3-9, it is possible to appreciate that the nadir frequency of both generators is lower the lower is the inertia of the machines.

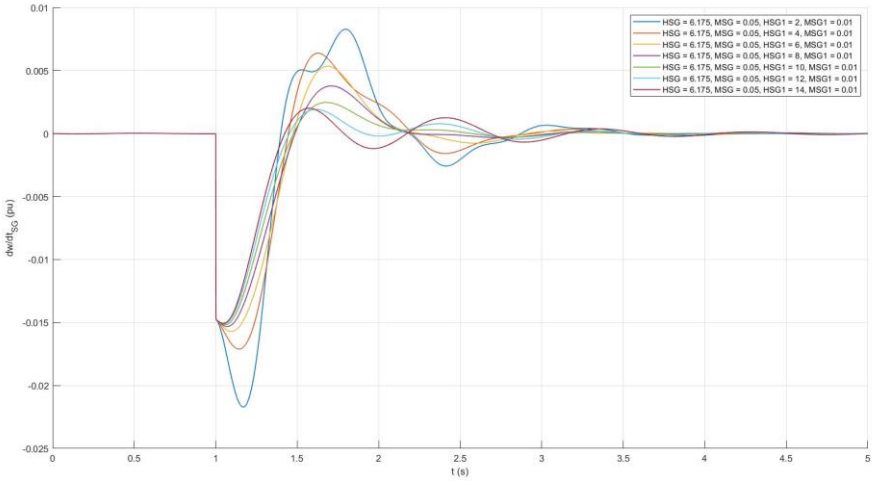

Figure 3.17: Frequency derivative of SG for different values of virtual inertia.

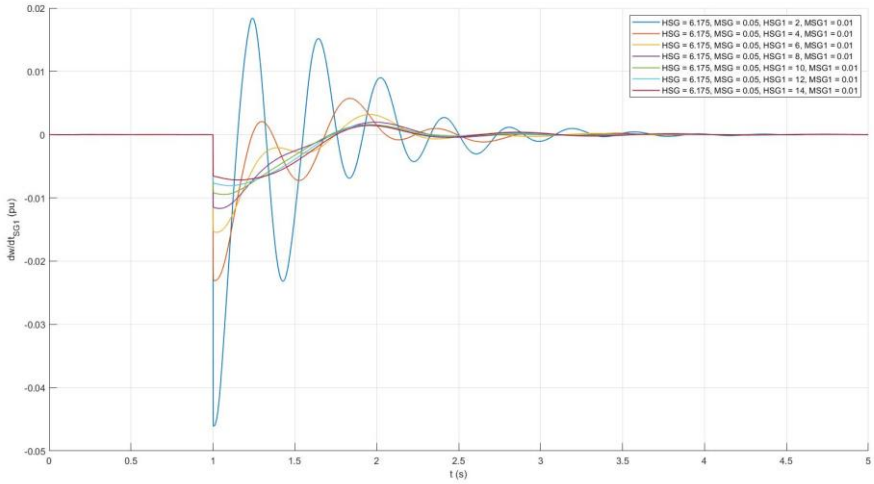

Figure 3.18: Frequency derivative of SG1 for different values of virtual inertia

Figure 3.17 and Figure 3.18 show the frequency derivative of both synchronous generators. As shown numerically in Table 3-10, the RoCoF of generator "SG" at the instant of failure is the same for all cases, while the maximum RocoF in absolute value varies depending on the inertia of generator "SG1" as we can check numerically in Table 3-9.

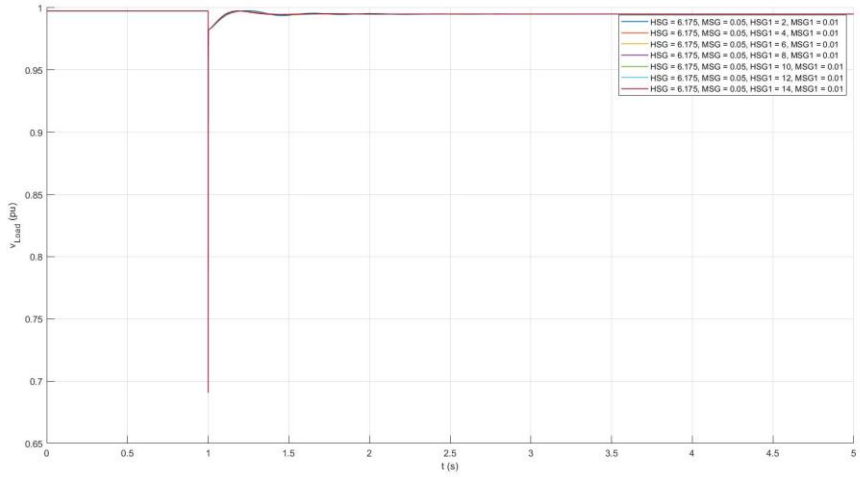

Figure 3.19: Load voltage for different values of virtual inertia.

H_{VSM} (s)	$\|RoCoF\|_{MAX,SG1}$(pu/s)	$\|RoCoF\|_{MAX,SG}$(pu/s)	$Nadir_{SG1}$	$Nadir_{SG}$
2	$46.11*10^{-3}$	$21.7*10^{-3}$	0.994659	0.993895
4	$23.06*10^{-3}$	$17.05*10^{-3}$	0.995529	0.994491
6	$15.34*10^{-3}$	$15.71*10^{-3}$	0.995907	0.994917
8	$11.44*10^{-3}$	$15.32*10^{-3}$	0.996069	0.995328
10	$9.18*10^{-3}$	$15.17*10^{-3}$	0.996121	0.99569
12	$7.65*10^{-3}$	$15.10*10^{-3}$	0.996171	0.995987
14	$6.49*10^{-3}$	$15.07*10^{-3}$	0.996235	0.996209

Table 3-9: Maximum RoCoF in absolute value and frequency nadir of both synchronous machines.

$\|RoCoF_{SG}\|_{t=1^+}$(pu/s)	f_{ss} (pu)
$14.67*10^{-3}$	0.996637

Table 3-10: RoCoF of SG at the instant of failure and frequency in steady state.

3.2.3 Study of the inertial response of the converter for current limit conditions

This test seeks to analyze the inertial behavior of the converter when it reaches the current limit that the transistors can withstand. This limit has been set in the current control so that the current provided by the converter saturates if I_{max} = 1.1 pu is reached. This test will be analyzed only for configuration 1 and for the same range of converter inertias studied in *test 2*. *Configuration 2 and 3* will not be studied in this test because for the same scenario that causes the converter to saturate, the generator loses synchronism and is not able to maintain stability in the grid. To avoid this loss of synchronism would require a synchronous machine with a capacity much higher than that of the converter, which makes no sense in this study where grids are assumed to be governed almost entirely by renewable energy sources.

- **Configuration 1**

To cause the converter to saturate once the fault occurs, different load scenarios have been simulated. In all of them the converter is made to work close to its power limit without initially saturating so that as soon as the fault occurs the converter reaches the limit. Figure 3.20 shows the frequency graphs for different power demand scenarios, all of them for the same generation step of 5 MW, and a single value of inertia and droop of the converter, specifically H_{VSM} = 7 s and M_{PVSM} = 0.01 pu, which have been shown to be stable values in the simulations.

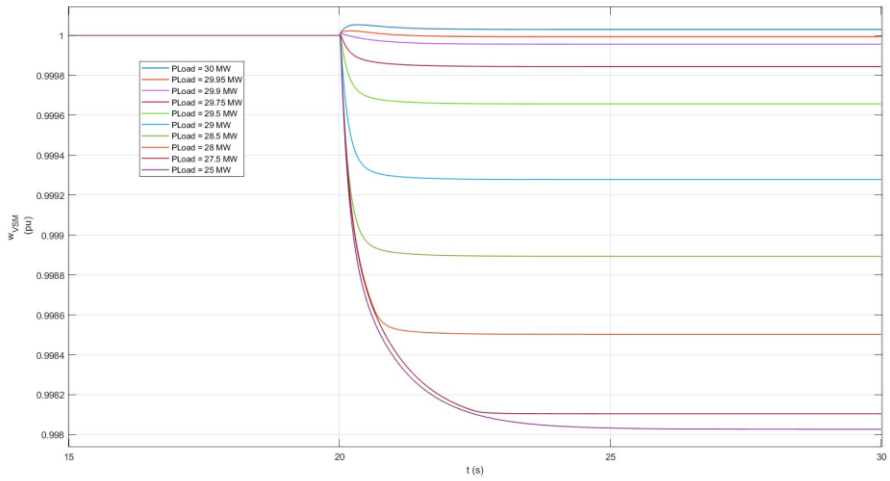

Figure 3.20: Frequency of the converter for current limit conditions.

As we can see in Figure 3.20, as we demand more power to the converter before the fault, the smaller the frequency step for the same power step and the same droop value. This is because the loss of generation at the instant of failure causes a peak in the voltage drop of the capacitor, as seen in Figure 3.7, which the converter must regulate. To control this voltage, the external voltage loop generates a reference current of the converter as shown in equations (2.9) and (2.10). This current, before being used as a reference for the internal current loop, passes through a limiting block

that saturates it in case it reaches the established limit, not allowing the reference voltage value to be reached. As the converter reaches the current limit earlier each time, the error in the voltage control keeps increasing. This error in the voltage regulation of the capacitor causes the power measured at the converter output to decrease each time, because the power demanded by the load depends quadratically on the voltage. This explains that the earlier the converter current saturates, the lower the voltage at the load and therefore the smaller the power and frequency step, exceeding 50 Hz in the most extreme cases, which means that the converter would be absorbing power.

Since it does not make sense to study the case in which the converter absorbs power because the voltage would be so low that the system would not be functional, we will choose a case which, despite not regulating the voltage completely, is at least capable of maintaining it at an acceptable value.

For this test we have chosen the scenario shown in Table 3-11, which allows to reach in steady state a capacitor voltage of 0.98 pu.

Δp	M_{PVSM}	P_{LOAD}	P_{LG}	S_{BVSM}
0.2 pu	0.01 pu	28 MW	5 MW	25 MVA

Table 3-11: Initial parameters used for test 3 - configuration 1.

The following measurements have been obtained for different converter inertia values:

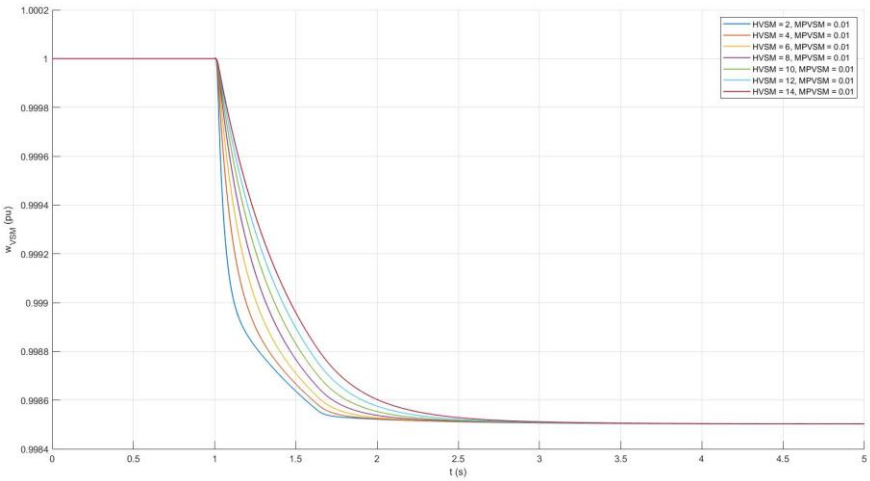

Figure 3.21: VSM frequency for different values of virtual inertia.

Figure 3.21 shows the frequency behavior of the converter at different values of the inertia constant. As we can see, despite having reached the saturation limit, the converter shows an inertial behavior similar to the one it had working under standard conditions seen in Figure 3.5 , although now it presents a more abrupt bend. The response still resembles a first order system response to an input step. In addition, both the nadir frequency and the steady-state frequency are included in Table 3-13.

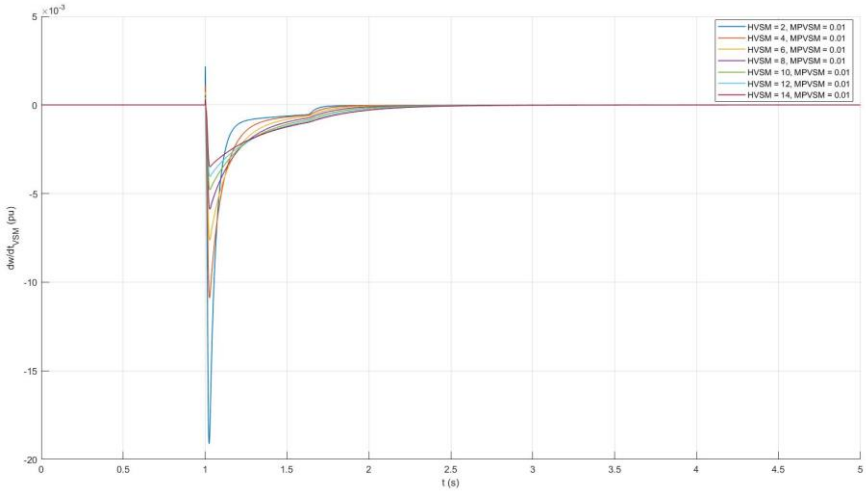

Figure 3.22: VSM frequency derivative for different inertia values.

Figure 3.22 shows the derivative of the frequency for the selected range of inertias. In this plot the abrupt changes in the derivative mentioned above can be seen more clearly. The different values of the maximum RoCoF in absolute value can also be observed. These values are specified in Table 3-12.

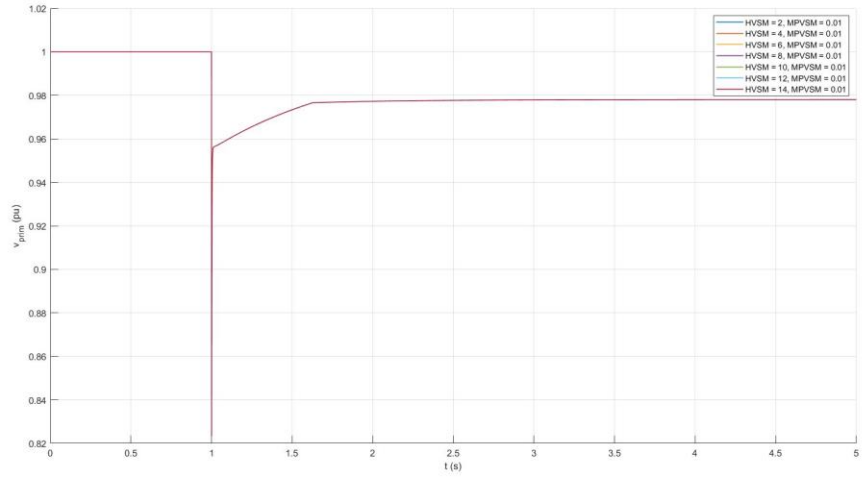

Figure 3.23: Capacitor voltage for different values of virtual inertia.

Figure 3.23 shows how the inverter is not able to regulate the capacitor voltage due to the current limit, causing a steady-state error in the voltage.

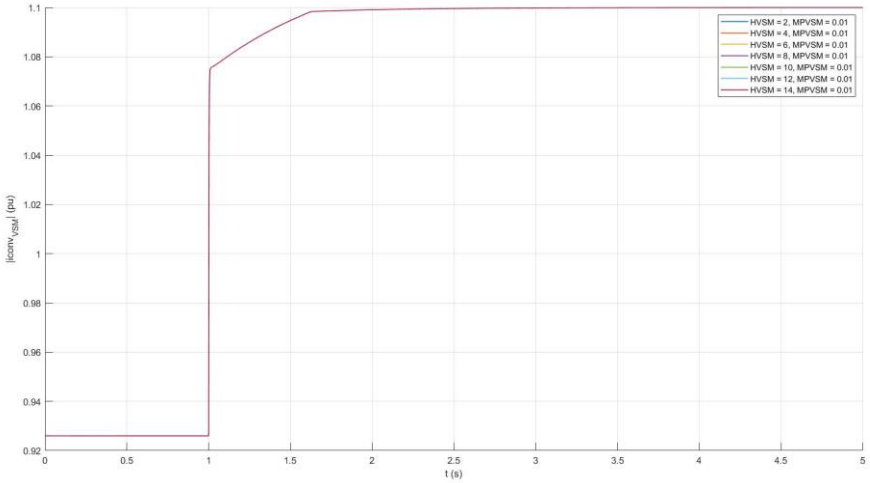

Figure 3.24: Current through the converter for different values of virtual inertia.

Figure 3.24 shows how the converter current saturates to its maximum allowable value (1.1 pu) when the failure occurs.

H_{VSM} (s)	$\|RoCoF\|_{MAX}$ (pu/s)
2	$19.1*10^{-3}$
4	$10.89*10^{-3}$
6	$7.63*10^{-3}$
8	$5.88*10^{-3}$
10	$4.78*10^{-3}$
12	$4.02*10^{-3}$
14	$3.49*10^{-3}$

Table 3-12: Maximum RoCoF in absolute value.

$Nadir_{VSM}$ (pu)	f_{ss} (pu)
0.998503	0.998503

Table 3-13: Frequency nadir and steady state frequency.

3.3 COMPARISON

3.3.1 Comparison between the inverter and the synchronous machine under standard conditions

Before comparing *tests 3.2.2 and 3.2.3* with each other, it is necessary to know the differences between the synchronous machine and the converter when operating under normal conditions.

The first thing to note is that the converter is modeled following the swing equation of the synchronous machine, which makes it present a frequency vs. power response of a first order system. While the synchronous generator modeled in Matlab includes in addition to the synchronous machine model a speed governor and a steam turbine that in this particular case is a fourth order system, which depending on the values of inertia and droop chosen is over damped or under damped, as can be seen in Figure 3.16.

In addition, another essential difference is the origin of the inertial response of both. The synchronous machine presents a real inertia that is defined as the resistance to the rotor speed variation when there is a variation in the torque, i.e. when the power varies the rotor slows down or accelerates maintaining the equilibrium. However, the way for the converter to mimic this behavior to a power variation is to measure the power delivered at each instant and control the frequency of the converter based on this measurement.

The problem is that this power measurement is made from the voltage and current at the output of the converter as explained in equations (2.28) and (2.29). Therefore,

voltage peaks cause power peaks and this causes improper behavior of a synchronous generator as can be seen in the zoom of Figure 3.11.

Another difference that is important to highlight is the origin of the so-called inertia constant that appears in the equations of the synchronous machine and that has its analog in the case of the inverter. In the case of the synchronous machine, the inertia constant depends on the masses and their distribution in the rotor, while the virtual inertia constant of the inverter is part of the time constant of a low-pass filter. This low pass filter models the synchronous machine equation in the Laplace domain. That is, the origin of the virtual inertia constant is purely mathematical. This explains that for different values of the inertia constant in Figure 3.5 one sees first-order responses with increasing time constant.

Finally, it should be noted that as can be seen if we compare the RoCoF of Table 3-6 and Table 3-7, the converter presents a higher inertial response than the synchronous machine for the same value of the inertia constant. This is not necessarily an advantage since the values of inertia and droop of the converter are very dependent on the characteristics of the grid being used.

3.3.2 Comparison between tests 3.2.2 and 3.2.3

In order to know the limitations that the converter suffers when working above its capacity, we will compare the last tests and explain the results obtained.

If we compare Table 3-3 and Table 3-4 with Table 3-12 and Table 3-13, it is possible to observe that the maximum RoCoF in absolute value is higher when the converter operates in standard conditions. This does not mean that the inertial response improves if the converter operates at the limit, but that the inertial response depends on the converter current in an indirect way. Specifically, the voltage control on the capacitor depends on the converter current, and as explained before, the power and therefore the frequency depend on the control of this voltage. Thus, limiting the

converter current limits the voltage, as shown in Figure 3.23, making the power variation smaller and consequently also the initial slope of the frequency.

This deduction leads to think that the synthetic inertial response of the converter is supported by a purely mathematical part which is the inertia constant and another physical part in the form of electrical energy whose origin is possibly the DC power source which is after all the one that provides the energy to regulate the flow of current from the converter to the grid.

Furthermore, if we compare Figure 3.6 and Figure 3.22, we can observe how when the inverter current is saturated at a constant value, the frequency derivative presents more abrupt variations the lower the inertia constant is. This is because, as mentioned above, the inertia constant is proportional to the time constant of the first-order system that models the VSM, which means that for small values of the inertia constant the response to equal variations in power is faster. For this reason, when H_{VSM} = 2 pu, we can appreciate an exponential response with a steep slope. This means that when the current limit is reached the frequency must correct its slope abruptly. This change in slope occurs for all inertia values, but in cases where the time constant is larger, the slope is smoother, and the correction is barely visible to the naked eye.

Chapter 4. CONCLUSIONS AND FUTURE WORK

4.1 CONCLUSIONS

This work aimed to implement a VSM control in Matlab/Simulink and to analyze the inertial response of the converter against disturbances in the grid when the converter works under normal conditions and when it reaches the current limit.

For this purpose, a VSM control has been designed in Simulink and different configurations of Grid Forming converters and synchronous machines have been simulated for different disturbances in the grid. These simulations consisted of isolating the converter alone or together with a synchronous machine from the grid, to feed a purely resistive load.

These objectives have been met and the following conclusions have been reached:

- As it has been verified the virtual inertia works correctly when the converter operates under normal conditions, it has a similar performance to a synchronous machine presenting even a flatter RoCoF for the same inertia values.
- When the current limit of the converter is reached the inertial response does not disappear but is affected by the converter's inability to regulate the grid voltage. Giving rise to an adjacent problem, which is the converter's dependence on regulating the capacitor voltage to provide an inertial response similar to that of a conventional synchronous machine. In addition, as a consequence of the converter limitation the frequency response ceases to resemble a first order system response and exhibits a sharp bend in its slope.
- The virtual inertia of the Grid Forming converter with VSM control is highly dependent on the voltage control of the LC filter capacitor. This can be a problem if the converter reaches the current limit when feeding voltage invariant loads.

4.2 FUTURE WORK

Based on this project, the following work can be developed in the future:

- Design more accurate voltage and current control parameters that do not cause problems in borderline cases.
- Perform the same study including a low-pass filter in the power measurement, which disappears as a consequence of designing a VSM model equivalent to the droop control. As explained in [12] the operation of the control without filter is of no practical use.
- Include a model of the converter with IGBT transistors generating the PWM signal from the reference converter voltage, to study the filter characteristics necessary to filter harmonics instead of using an ideal three-phase current source.
- Model in Matlab a system whose load is independent of voltage to study the behavior of the converter's inertial response to this type of load, which has been shown to be a problem.

In general, make a more realistic design of the model and study its performance in different grid cases.

Chapter 5. ALIGNMENT WITH THE SUSTAINABLE DEVELOPMENT GOALS

In 2015, the UN defined seventeen goals to protect and improve the planet by 2030. Two of them are aligned with the goals of this project.

- **Affordable and clean energy (Objective 7):** The introduction of renewable energies in weak grids has started to reach its limit due to the decrease in stability of the grid because of the replacement of conventional SMs by PVs and wind turbines. This project focuses on the study of converters that try to solve this problem.
- **Industry, Innovation, and Infrastructure (Objective 9):** The study of this type of converters is not a topic that has been widely addressed in the literature and their behavior under limited conditions is still not fully known. This is why this project is related to the innovation and investigation objective.

Chapter 6. BIBLIOGRAPHY

[1] Ebrahim Rokrok; Taoufik Qoria; Antoine Bruyere; Bruno Francois; Xavier Guillaud, “Classification and Dynamic Assessment of Droop-Based Grid-Forming Control Schemes: Application in HVDC Systems” Electric Power Systems Research, ISSN: 0378-7796, Vol: 189, Page: 106765, 2020.

[2] T. Qoria, E. Rokrok, A. Bruyere, B. François and X. Guillaud, "A PLL-Free Grid-Forming Control With Decoupled Functionalities for High-Power Transmission System Applications," in IEEE Access, vol. 8, pp. 197363-197378, 2020, doi: 10.1109/ACCESS.2020.3034149.

[3] G. Denis, "From grid-following to grid-forming: The new strategy to build 100% power-electronics interfaced transmission system with enhanced transient behavior", 2017.

[4] F. Milano, F. Dorfler, G. Hug, D. J. Hill and G. Verbic, "Foundations and challenges of low-inertia systems (Invited Paper)", *Proc. Power Syst. Comput. Conf. (PSCC)*, pp. 1-25, Jun. 2018.

[5] S. D'Arco and J. A. Suul, "Equivalence of Virtual Synchronous Machines and Frequency-Droops for Converter-Based MicroGrids," in IEEE Transactions on Smart Grid, vol. 5, no. 1, pp. 394-395, Jan. 2014, doi: 10.1109/TSG.2013.228800.

[6] Taoufik Qoria, François Gruson, Frédéric Colas, Guillaume Denis, T. Prevost, et al.. Inertia effect and load sharing capability of grid forming converters connected to a transmission grid. The 15th IET international conference on AC and DC Power Transmission, Feb 2019, Coventry, United Kingdom. pp.6. ffhal-02082462.

[7] Qoria, T., Cossart, Q., Li, C., Guillaud, X., Colas, F., Gruson, F., & Kestelyn, X. (2018). WP3-Control and Operation of a Grid with 100% Converter-Based Devices. Deliverable 3.2: Local control and simulation tools for large transmission systems. *MIGRATE Project*.

[8] Harrison, S., Henderson, C., Papadopoulos, P. N., & Egea-Alvarez, A. (2021). Assessment of droop and VSM equivalence considering the cascaded control dynamics.

[9] R. Ofir, U. Markovic, P. Aristidou and G. Hug, "Droop vs. virtual inertia: Comparison from the perspective of converter operation mode," 2018 IEEE International Energy

Conference (ENERGYCON), Limassol, Cyprus, 2018, pp. 1-6, doi: 10.1109/ENERGYCON.2018.8398752.

[10] García, A., Ortega, Á., Rouco, L., & Sigrist, L. (2021). FLEXENER–TECHNICAL REPORT.

[11] LOPES, João Peças; HATZIARGYRIOU, N.; SARAIVA, João Tomé. Management of microgrids. 2003.

[12] HU, Wenqiang; WU, Zaijun; DINAVAHI, Venkata. Dynamic analysis and model order reduction of virtual synchronous machine based microgrid. IEEE Access, 2020, vol. 8, p. 106585-106600.

[13] Unruh, P., Nuschke, M., Strauß, P., & Welck, F. (2020). Overview on grid-forming inverter control methods. *Energies*, *13*(10), 2589.

[14] ALOIS, Informe E21 – "Sistema de control y protección de Alimentadores reales de media tensión para una Operación en Isla estable y sostenible en el tiempo", 2017